HIGH ENERGY PULSED LIQUID LASER

H. Samelson, et al

GTE Laboratories, Incorporated

Prepared for:

Office of Naval Research

31 August 1973

HIGH ENERGY PULSED LIQUID LASER

Semiannual Technical Summary Report

U. S. Navy, Office of Naval Research
Washington, D. C.
Contract N00014-68-C-0110

31 August 1973
TR 73-826.4

Sponsored by
Advanced Research Projects Agency
ARPA Order No. 1806, Amendment No. 9

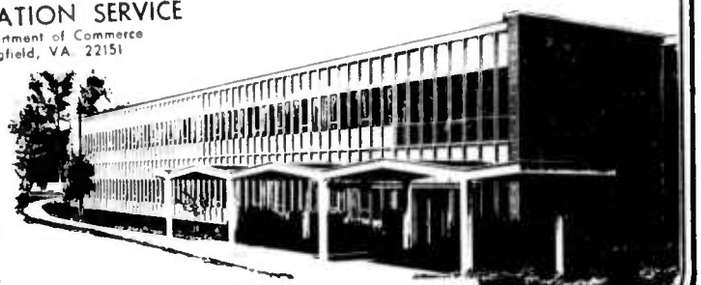

GTE LABORATORIES
INCORPORATED
Waltham, Massachusetts 02154

UNCLASSIFIED

SECURITY CLASSIFICATION OF THIS PAGE (When Data Entered)

REPORT DOCUMENTATION PAGE		READ INSTRUCTIONS BEFORE COMPLETING FORM
1. REPORT NUMBER	2. GOVT ACCESSION NO.	3. RECIPIENT'S CATALOG NUMBER
4. TITLE (and Subtitle) HIGH ENERGY PULSED LIQUID LASER		5. TYPE OF REPORT & PERIOD COVERED Semiannual Technical Summary 1 February - 31 July 1973
		6. PERFORMING ORG. REPORT NUMBER TR 73-826.4
7. AUTHOR(s) H. Samelson, R. Kocher, A. Lempicki		8. CONTRACT OR GRANT NUMBER(s) N00014-68-C-0110
9. PERFORMING ORGANIZATION NAME AND ADDRESS CTE Laboratories Incorporated 40 Sylvan Road Waltham, Mass. 02154		10. PROGRAM ELEMENT, PROJECT, TASK AREA & WORK UNIT NUMBERS ARPA No. 1806, Amendment No. 9
11. CONTROLLING OFFICE NAME AND ADDRESS U. S. Navy Office of Naval Research Washington, D.C.		12. REPORT DATE 31 August 1973
		13. NUMBER OF PAGES 82
14. MONITORING AGENCY NAME & ADDRESS(if different from Controlling Office) Same as block 11.		15. SECURITY CLASS. (of this report) Unclassified
		15a. DECLASSIFICATION/DOWNGRADING SCHEDULE

16. DISTRIBUTION STATEMENT (of this Report)

Qualified requestors may obtain copies of this report from DDC.

DISTRIBUTION STATEMENT A
Approved for public release;
Distribution Unlimited

17. DISTRIBUTION STATEMENT (of the abstract entered in Block 20, if different from Report)

18. SUPPLEMENTARY NOTES

19. KEY WORDS (Continue on reverse side if necessary and identify by block number)

Neodymium liquid laser; high average power laser; hydrodynamic model

20. ABSTRACT (Continue on reverse side if necessary and identify by block number)

Significant advances have been made in both the performance and understanding of liquid lasers. High average powers in excess of 400 watts at 5 pps have been obtained during the course of the work. Some scaling laws in terms of the relationship between active volume and power loading have emerged. Finally, a large body of information relating steady-state laser performance to imposed thermal gradients has been obtained, and a method has been devised for reducing the data so that the information it contains is readily displayed.

DD FORM 1 JAN 73 1473 EDITION OF 1 NOV 65 IS OBSOLETE

UNCLASSIFIED

SECURITY CLASSIFICATION OF THIS PAGE (When Data Entered)

20. In addition, a hydrodynamic model for the liquid in turbulent flow under various temperature differentials has been obtained. This model provides detailed information on the radial thermal gradient. Under the special condition of extrapolation to zero power input, the model can be related to the experiment and significant information on the nature and the effect of the thermal gradient on laser performance. The picture that emerges from this is then qualitatively extended to the case of high average power loading.

The information on the thermal gradient is applied to provide a treatment of the optical behavior of the flowing liquid. From this an estimate of the distortion of a propagated wave is made, and it is shown that, in a single pass, the path length change across the effective aperture of the laser is about one wavelength.

HIGH-ENERGY PULSED LIQUID LASER

Contract No. N00014-68-C-0110

ARPA Order Number:	1806, Amendment No. 9	Date of Report:	31 August 1973
Project Code Number:	421	Contract Expiration Date:	31 December 1973
Date of Contract:	1 July 1967	Project Scientist:	H. Samelson
Amount of Contract:	$654,603.00	Telephone:	617-890-8460

ACKNOWLEDGMENT

This research was supported by the Advanced Research Projects Agency of the Department of Defense and was monitored by the Office of Naval Research under Contract No. N00014-68-C-0110.

DISCLAIMER

The views and conclusions contained in this document are those of the authors and should not be interpreted as necessarily representing the official policies, either expressed or implied, of the Advanced Research Projects Agency or the U. S. Government.

GTE LABORATORIES INCORPORATED
Waltham, Massachusetts 02154

ABSTRACT

Significant advances have been made in both the performance and understanding of liquid lasers. High average powers in excess of 400 watts at 5 pps have been obtained during the course of the work. Some sealing laws in terms of the relationship between aetive volumc and power loading have emerged. Finally, a large body of information relating steady-state laser performance to imposed thermal gradients has been obtained, and a method has been devised for reducing the data so that the information it eontains is readily displayed.

In addition, a hydrodynamic model for the liquid in turbulent flow under various temperature differentials has been obtained. This model provides detailed information on the radial thermal gradient. Under the speeial condition of extrapolation to zero power input, the model can be related to the experiment and signifieant information on the nature and the effect of the thermal gradient on laser performance. The picture that emerges from this is then qualitatively extended to the case of high average power loading.

The information on the thermal gradient is applied to provide a treatment of the optical behavior of the flowing liquid. From this an estimate of the distortion of a propagated wave is made, and it is shown that, in a single pass, the path length ehange across the effective aperture of the laser is about one wavelength.

CONTENTS

ILLUSTRATIONS

Preceding page blank

ILLUSTRATIONS (Continued)

ILLUSTRATIONS (Continued)

SUMMARY

The principal emphasis of the work performed during the present reporting period was:

1) To develop a useful hydrodynamic model for the laser liquid in turbulent flow.

2) To check out the overall performance of the new design feature and new components.

3) To determine the laser performance characteristics of the new system.

We have had considerable success in applying hydrodynamic considerations to the flow problem. The approach used was to adapt a treatment previously used by Martinelli for the flow of molten salts in pipes. As shown in Section 2, this can be done, and the results are applicable to the case where there is a temperature differential between the circulating liquid and the outer pipe wall, and there is no heat source in the flowing liquid. The basic information obtained from this model is the radial temperature gradient.

In Section 3, the radial temperature gradient is specifically obtained for the case of the laser liquid. It is then used to describe the optical properties of the laser liquid. It is shown that a ray, propagating off the centerline of the cylindrical cell, will be deviated. This deviation increases with increasing temperature gradient, that is, with increasing distance from the cylinder axis. There are two consequences of this: first, the magnitude of the deviation will ultimately vignette the effective laser aperture; and second, there will be a change in path length for the single pass propagation of a wave as in an amplifier application. In the latter case, given the gradient and effective aperture, the path length change can be calculated.

Section 4 presents a description of the laser system from the point of view of design and construction. Here we present detailed information on cell design, circulating pump characteristics, the power supply, the cooling system and the pulse forming networks.

The actual experimental results are given in Section 5. These deal with the relation between output energy and input energy and the system parameters: flow speed or Reynolds number, and the controlled temperature differential between the laser liquid and the external water coolant of the cell. The parameter used to characterize the output is E/E_0 where E is the pulse output energy of the repetitive train of pulses

after the steady state has developed and E_0 is the single-shot pulse output energy with a zero temperature differential. The independent variable in the experiment is the average power input. The extrapolated value of E/E_0 at zero power input decreases with increasing ΔT. In general, E/E_0 passes through a maximum when plotted as a function of average power input. The average input power at which the maximum occurs increases with increasing Reynolds number and temperature differential.

We have been able to use the zero input power information to establish the quantitative validity of the hydrodynamic model and relate the model to experiment. On the basis of the applicability of the model we discuss a qualitative extension to those cases where power is put into the laser.

The dynamic loss of the laser material has been determined and is between 0.2 and 0.6% per cm depending on the method of measurement used. From the loss and threshold data the small signal gain is approximately 20 dB per pass at 4000 J input, and this appears to be adequate for the amplifier work.

The future plans related to the amplifier and beam distortion measurements are briefly discussed in Section 6.

1. INTRODUCTION

The objectives of the High Energy Pulsed Liquid Laser project are related to long pulse oscillator performance and short pulse, high-brightness operation. The latter objective is, at this point, more significant and the operational goal is an output between 25 and 50 watts average power at a repetition rate of 5 pulses per second. The output beam will consist of Q-switched pulses of about 50 ns duration, and the beam shall be diffraction limited or as close thereto as possible.

The long pulse work has resulted in performance in excess of 400 watts average power at 5 pps. This was obtained with a limited and conservative operation of the power supply and flash lamps and an ultimate performance between 25 and 50% higher is feasible. However, this was not pursued because the information relevant to the objectives could be obtained at the more restricted power input levels. This long pulse information is important to the understanding of the thermal-hydrodynamic state of the gain medium during repetitive pulse excitation, as well as defining small-signal gain performance of the system.

The main thrusts of the work reported here are twofold. First, there is the development of a hydrodynamic model which leads to an evaluation of the radial thermal gradient in the circulating liquid. Basically the equations for turbulent flow are solved for the boundary conditions that the liquid has one bulk temperature and the external wall of the tube (cell) has another. A consideration of energy and momentum transfer in the turbulent liquid leads to the expression for the radial thermal gradient. This is considered in Sections 2 and 3. In Section 3, we also consider the optical consequences of the radial thermal gradient and show that for a single pass the optical distortion, over a rather large aperture of the active medium, is quite small.

The second part of the work to be discussed concerns the long pulse laser work. First, in Section 4, the apparatus is described. Then, in Section 5, the detailed experimental work is presented. This covers the long pulse laser output under different conditions of flow, power input and temperature differential. Part of these results can be correlated with the model set up earlier and tend to confirm the results of the calculation. The overall output behavior is then qualitatively described by an extension of the model.

Finally, in Section 6, we briefly outline the next phase of the work.

2. HYDRODYNAMIC ANALYSIS OF THE LASER LIQUID

In a liquid laser, in which the active medium is transported through a tubular cell, there is both a radial velocity and temperature gradient. When the temperatures of the circulating liquid and the environment external to the cell are the same, the radial thermal gradient vanishes. However, on optical excitation of the laser, either pulsed or cw, the isothermal character is destroyed and a radial thermal gradient will arise. If the laser cavity is optimally adjusted for isothermal performance, this thermal gradient will result in a degraded output. To correct for this, one may optically compensate the laser resonator[1] or, as is more commonly done, cool the laser medium.

The cooling and temperature control of the active medium is more readily accomplished in the case of a liquid. In this section we shall present a model for a laser cell with a circulating laser liquid and present a hydrodynamic analysis which ultimately results in an expression for the radial temperature profile across the laser cell. The solution is limited to the case where there is no input power (optical excitation) but with the bulk laser liquid at a temperature different from the laser cell wall. In a later section the analysis of experimental data will enable us to make contact with the calculation and to provide the basis for a qualitative extension to the cases where there is substantial power input.

The Hydrodynamic Model

The analysis of the thermal characteristics of a liquid laser is based on the hydrodynamics of the circulating liquid. In detail, we are interested in temperature distribution of a fluid under turbulent flow through a pipe. The experimental laser cell to which the analysis is to be applied is illustrated in Figure 1(a). The region to be considered is the active length L, of inside diameter D, between the interior faces of the cell windows. A section of the cell is shown in Figure 1(b). The bulk circulating laser liquid is maintained at a temperature T_{CL} which is assumed to be the temperature at the centerline of the cell ($r = 0$) and the cooling water is maintained at a temperature T_0.

The hydrodynamic analysis of turbulent flow is very complicated and the results, in general, are semiempirical in nature. The more manageable results are obtained for the case of a fully developed flow which is established some distance after the liquid has entered the pipe.[2] A value of 10D is a rough measure of this distance and $L > 10D$

Preceding page blank

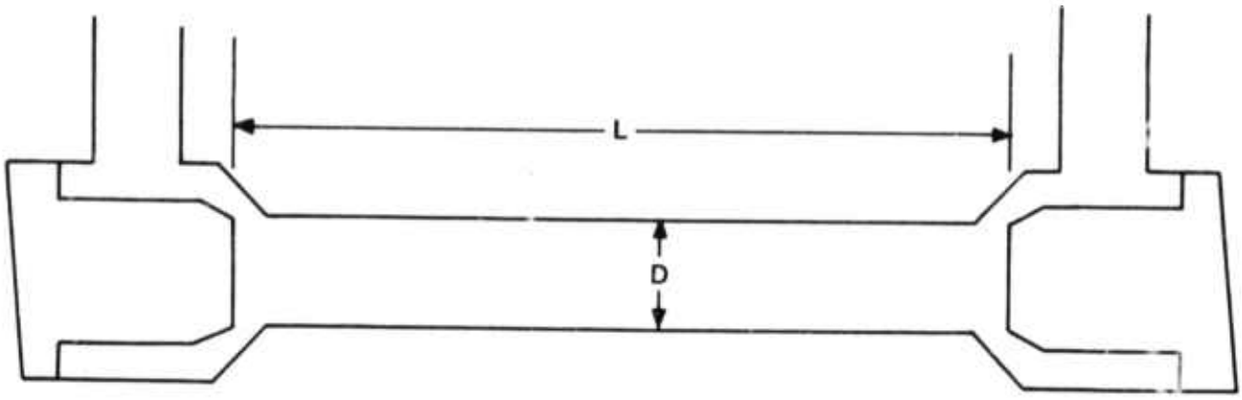

(a) Side View (Without Water Jacket).

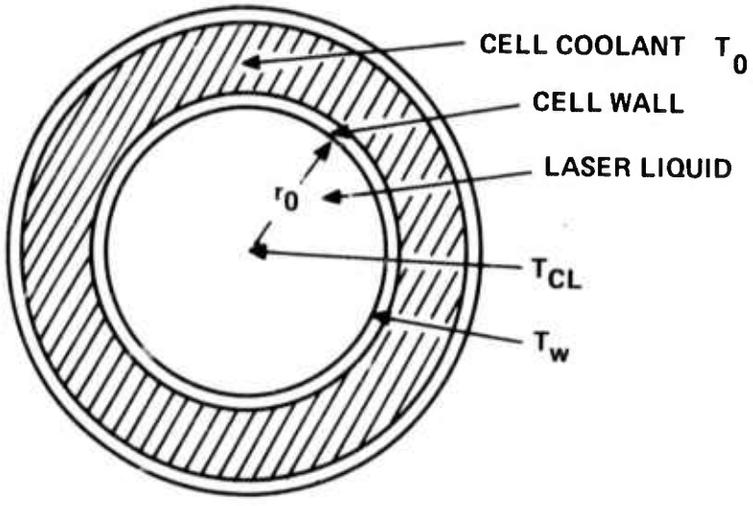

(b) Cross Section Showing Water Jacket.

Figure 1. Schematic Drawings of a Water-Jacketed Laser Cell.

is not satisfied in some of the experimental cases to be discussed. However, the plenum chamber of the laser cell has a tapered entry into the cell pipe, and this assists the rapid establishment of a fully developed flow. We assume for simplicity that in all cases there is fully developed flow throughout the active region of the laser cell.

For fully developed flow, the average velocity in the axial (z) direction at any radius r is independent of time, distance down the tube (z) and angular position in the tube. In addition, the mean radial velocity, v(r) is zero but there are nonzero fluctuations of velocity, v_r amd v_z, in the radial and axial directions, respectively. Hence, the mean flow in the axial direction, u(z), is one dimensional but the turbulent fluctuations at any point are two dimensional.

For such a system, since the liquid is incompressible, the pertinent equations are the Navier-Stokes equation (with no body forces):

$$\mu\nabla^2 \vec{v} = \nabla p + \rho \vec{v} \cdot \nabla\vec{v} + \frac{\partial \vec{v}}{\partial t} \tag{1}$$

and the equation of continuity:

$$\rho \bar{v} \cdot \vec{v} = 0 \tag{2}$$

where μ is the dynamic viscosity, p the pressure and ρ the density. In addition, there is the energy balance equation:

$$k\nabla^2 T = \rho C_p (v \cdot \nabla T) + \frac{\partial T}{\partial t} \tag{3}$$

where T is the temperature, C_p the heat capacity, and k the thermal conductivity. The conditions of turbulent flow are introduced into the problem by Eq. (4) which states that the instantaneous value of quantity in a turbulent flow field is given by the mean value (the barred quantity) and a fluctuating part (the primed quantity):

$$\begin{aligned} v &= \bar{v} + v' \\ T &= \bar{T} + T' \\ p &= \bar{p} + p' \end{aligned} \tag{4}$$

Equations (1) and (3) undergo considerable simplification when the conditions of steady state and fully developed flow are imposed. For flow in a pipe we then have

that $\vec{v}$ and T are functions of r only and the time derivatives are zero. Then, putting Eq. (4) into Eqs. (1) and (3) and using the continuity equation, [Eq. (2)], and the fact that the time averages of the primed quantities are zero, we obtain the time averaged equations:

$$\frac{1}{\rho}\frac{\partial p}{\partial z} + \frac{1}{r}\frac{\partial}{\partial r} r\left[v'_r v'_z - \nu \frac{\partial v}{\partial r}\right] = 0 \tag{5}$$

and

$$\frac{\partial T}{\partial z} + \frac{1}{r}\frac{\partial}{\partial r} r\left[v'_r T' - \alpha \frac{\partial T}{\partial r}\right] = 0 \tag{6}$$

where the unprimed quantities are the mean values [(the barred quantities in Eq. (4)] and $\nu = \frac{\mu}{\rho}$ and $\alpha = \frac{k}{\rho C_p}$. In Eq. (5), the first term represents the pressure forces, the second represents the forces arising from turbulent fluctuations, and the last represents viscous shear forces. In Eq. (6), the first term represents heat transport by convection, the second, heat transfer due to turbulent fluctuations, and the last represents heat transfer by molecular conduction.

The quantities involved in the radial derivatives of Eqs. (5) and (6) are apparent fluxes of momentum and heat. The first component in each case is a quantity arising from the turbulent nature of the flow while the second component is identical to that found in laminar flow alone. Using Prandtl's concept of eddy diffusivity, we can define:

$$-\left(\overline{v'_r T'}\right) = \epsilon_h \frac{\partial T}{\partial r} \tag{7}$$

and

$$-\left(\overline{v'_r v'_z}\right) = \epsilon_m \frac{\partial v}{\partial r}$$

so that Eqs. (5) and (6) become:

$$\frac{1}{\rho}\frac{\partial p}{\partial z} = \frac{1}{r}\frac{\partial}{\partial r}\left[r\left(\epsilon_m + \nu\right)\frac{\partial v}{\partial r}\right] \tag{8}$$

and

$$v\frac{\partial T}{\partial z} = \frac{1}{r}\frac{\partial}{\partial r}\left[r\left(\epsilon_h + \alpha\right)\frac{\partial T}{\partial r}\right] \tag{9}$$

The simultaneous solution of Eqs. (8) and (9) will provide the temperature distribution in the flowing liquid. Integrating (8), we have:

$$\frac{d}{dr}\left[r\left(\epsilon_m + \nu\right)\frac{dv}{dr}\right] = \frac{r}{\rho}\frac{dp}{dz}$$

At the wall $\epsilon_m = 0$ and $\frac{\tau_0}{\rho} = -\nu\frac{\partial v}{\partial r}\Big|_{r_0}$ where τ_0 is the shear stress of the fluid acting on the tube wall. Then,

$$+\frac{d}{dr}\left[r\frac{\tau_0}{\rho}\right] = -\frac{r}{\rho}\frac{dp}{dz}$$

$$r_0\frac{\tau}{\rho} = \frac{r_0^2}{2\rho}\frac{dp}{dz}$$

or

$$-\frac{1}{\rho}\frac{dp}{dz} = \frac{2\tau_0}{\rho r_0}$$

The general integral is

$$r\left(\epsilon_m + \nu\right)\frac{dv}{dr} = \int\frac{r}{\rho}\cdot\frac{dp}{dz}\cdot dr = -\frac{2\tau_0}{\rho r_0}\int r dr = -\frac{\tau_0}{\rho}\left(\frac{1}{2}\frac{2}{r_0}\right)$$

$$-\left(\epsilon_m + \nu\right)\frac{dv}{dv} = \frac{\tau_0}{\rho}\left(\frac{r}{r_0}\right)$$

or,

$$\left(\epsilon_m + \nu\right)\frac{dv}{dy} = \frac{\tau_0}{\rho}\left(1 - \frac{y}{r_0}\right) \tag{10}$$

where $y = r_0 - r$.

Similarly, a consideration of the heat flow Eq. (9) leads to the equation:

$$\frac{\left(q/A\right)_0}{\rho c_p}\left(1 - \frac{y}{r_0}\right) = -\left(\alpha + \epsilon_h\right)\frac{dT}{dy} \tag{11}$$

where $\left(q/A\right)_0$ is the heat flux from the wall into the fluid.

Equations (10) and (11) are formally similar in the variables v and T. Dividing (11) by (10) leads to a differential equation for $\frac{dT}{dy}$ in terms of $\frac{dv}{dy}$, other material and system constants and the ratio $\frac{\alpha + \epsilon_h}{\nu + \epsilon_m}$. These equations may be integrated by assuming an explicit form for the flow velocity field v(y). For this purpose, a modified form of the "universal velocity distribution" due to Von Kármán[3] is used as defined below:

$$v^+ = y^+ \qquad 0 \le y^+ \le 5$$

$$v^+ = 5.0 \ln y^+ - 3.05 \qquad 5 \le y^+ \le 30$$

$$v^+ = 5.5 + 2.5 \ln y^+ \qquad 30 \le y^+ \le \frac{y_0^+}{2}$$

$$v^+ = 6.75 + 2.5 \ln \frac{y_0^+}{2} - 5\left(1 - \frac{y^+}{y_0^+}\right)^2 \qquad \frac{y_0^+}{2} \le y^+ \le y_0^+$$

where

$$v^+ = \frac{v}{\sqrt{\tau_0/\rho}}$$

$$y^+ = \frac{1}{\nu}(r_0 - r)\sqrt{\frac{\tau_0}{\rho}}$$

$$y_0^+ = \frac{1}{\nu}\sqrt{\frac{\tau_0}{\rho}}\, r_0$$

The four regions of application of this function have historically been defined as, respectively, the laminar sublayer (near the wall), the buffer or transition sublayer, the turbulent sublayer and the core. In the latter two regions, $\epsilon_h >> \alpha$ and $\epsilon_m >> \nu$, and the ratio ϵ_h/ϵ_m is designated as E. Experimental values of E range from 0.9 to 1.7 and, in the absence of detailed information, a value of E = 1 is generally assumed. In the laminar sublayer, flow is governed by viscous forces and α and ν dominate to the degree where we can neglect ϵ_h and ϵ_m. In the buffer sublayer, all four quantities, ϵ_h, α, ϵ_m, and ν, must be retained.

The actual integration of first (10) and then (11) for each of the four regions will not be shown here for brevity. The interested reader is referred to the original paper by R. Martinelli[4] for the details in the first three regions. By extension of these calculations, the calculation of the core distributions is straightforward. The result of these calculations is, therefore, an explicit expression for the radial temperature distribution for a liquid flowing through a pipe with centerline temperature T_{CL} and wall temperature T_w. The following equations display this distribution:

$$\frac{T_{CL} - T(r)}{T_{CL} - T_w} = 1 - \frac{Pr.\left(y/y_1\right)}{D} \qquad 0 \le y = r_0 - r \le y_1 \quad (12)$$

$$= 1 - \frac{Pr + \ell n\left[1 + Pr\left(\frac{y}{y_1} - 1\right)\right]}{D} \qquad y_1 \le y \le y_2 \quad (13)$$

$$= 1 - \frac{Pr + \ell n\,(1 + 5\,Pr) + 0.5\,\ell n\left[\frac{Re}{30}\sqrt{\frac{f}{8}}\cdot\left(\frac{y}{r_0}\right)\right]}{D} \qquad y_2 \le y \le \frac{r_0}{2} \quad (14)$$

$$= 1 - \frac{Pr + \ell n\,(1 + 5\,Pr) + 0.5\,\ell n\left[\frac{Re}{60}\sqrt{\frac{f}{8}}\right] + \left[0.25 - \left(1 - \frac{y}{r_0}\right)^2\right]}{D} \qquad \frac{r_0}{2} \le y \le r_0 \quad (15)$$

where

Pr = Prandtl number $= \frac{\nu}{\alpha}$ (10 for the laser liquid used)

$$y_1 = \frac{10\,r_0}{(0.198)\,Re^{7/8}}$$

$$y_2 = 6y_1$$

Re = Reynolds number of flow $= \frac{v_{max}\left(2r_0\right)}{\nu}$

$$D = Pr + \ell n\,(1 + 5\,Pr) + 0.5\,\ell n\left[\frac{Re}{60}\sqrt{\frac{f}{8}}\right] + 0.25$$

Equations (12) to (15) and the subsequent definitions, obtained from the Martinelli analysis, allow the calculation of the temperature distribution of the flowing laser liquid in the cell as a function of the radius. These results apply to the case when there is a constant temperature difference between the center line (T_{CL}) and inner wall (T_w) temperature. The results are not applicable to the case where the centerline temperature is varying due to the addition of heat from an external source (flash lamps).

3. APPLICATION OF THE HYDRODYNAMIC SOLUTION TO THE LIQUID LASER

The solution to the hydrodynamic problem for the temperature distribution of a liquid flowing in a pipe is given by Eqs. (12) to (15), in which the solution is expressed in terms of the centerline temperature and the inner wall temperature. A typical example of what such a distribution might look like is shown in Figure 2. The centerline temperature is reasonably well-approximated by the bulk temperature of the flowing liquid; the inner wall temperature is more difficult to determine. Referring to Figures 1(b) and 2, it is seen that, in addition to the bulk laser liquid temperature, the only other temperature that is readily measured and known is that of the external cell coolant, T_0. The first problem, then, is to estimate T_w in terms of T_{CL}, T_0 and the flow characteristics. The knowledge of T_w enables us to apply Eqs. (12) to (15) and obtain the temperature distribution. The next task is to convert the temperature distribution to the index of refraction gradient and relate it to the optical behavior of the laser.

3.1 THE INNER WALL TEMPERATURE, T_w

If there is no external heat source, the radial flow of heat is determined by the temperature difference $T_{CL} - T_0$ and the volume flow rate through the cell. At the boundary between the liquid and the cell (inner cell wall) there will exist a temperature which, in the steady state, is determined by the heat arriving at the cell wall by forced convection from the liquid and the conductive heat flow through the cell wall.

For the latter we can write:

$$\frac{dQ}{dt} = - K_w A \frac{dT}{dx} \tag{16}$$

where

$\frac{dQ}{dt}$ = the heat flow per unit time

K_w = the thermal conductivity of the pyrex cell wall

A = the surface area

$\frac{dT}{dx}$ = the temperature gradient in the wall at the interface.

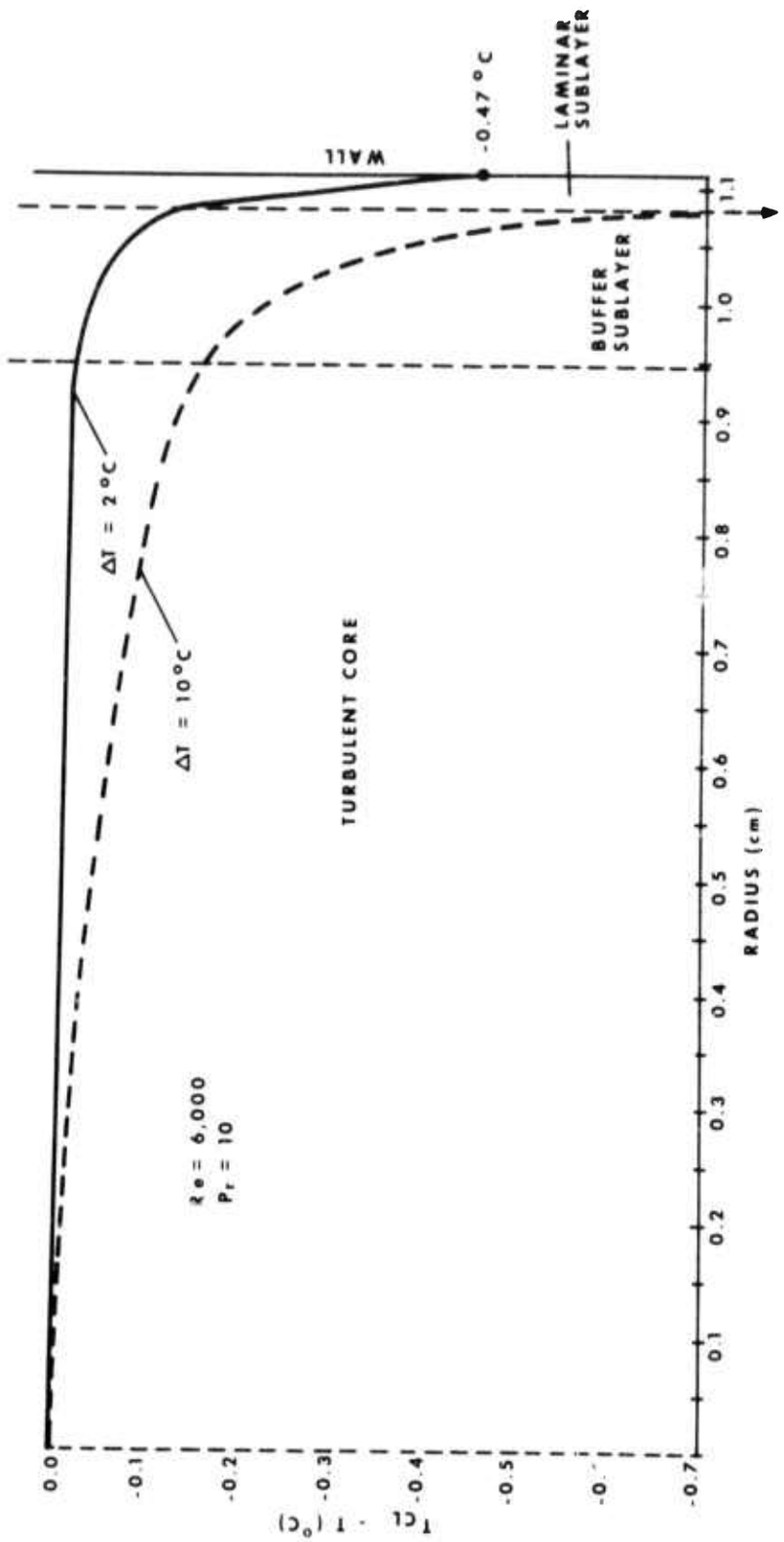

Figure 2. Typical Radial Temperature Profiles in the Liquid Laser Cell. Two values of $\Delta T = T_{CL} - T_0$ are shown. In this case, Re = 6,000, $r_0 = 1$, Pr = 10.

The flat plate approximation used here is valid since $\frac{r_0+t}{r_0} < 1.4$,[5] where t is the cell wall thickness. This can be rewritten as:

$$\frac{dQ}{Adt} = - K_w \frac{T_w - T_0}{t} \tag{17}$$

The heat transfer under forced convection from the laser liquid to the cell wall can be approximated by the calculation[6] of the Nusseult number, Nu:

$$Nu = \frac{hr_0}{K_L} \cong 0.027 \, (Re)^{0.8} \, (Pr)^{1/3} \tag{18}$$

where the surface heat transfer coefficient, h, is defined as:

$$h = \frac{dQ/dt}{A(T_{CL} - T_w)} = \frac{dQ/dt}{2\pi r_0 L(T_{CL} - T_w)} \tag{19}$$

and K_L is the thermal conductivity of the laser liquid. Combining (18) and (19) and using Pr = 10 for the laser liquid, we obtain:

$$\frac{dQ}{Adt}\Big|_{liquid} = K_L \beta \left(\frac{T_{CL} - T_w}{r_0} \right) \tag{20}$$

where $\beta = 5.82 \times 10^{-2} \, Re^{0.8}$. In the steady state the rate at which heat arrives at the wall [Eq. (20)] equals the rate at which it is transmitted through the wall [Eq. (17)]. Hence, equating (17) and (20), T_w is found to be:

$$T_w - T_0 = (T_{CL} - T_0) \left(\frac{\beta K_L / r_0}{\beta K_L / r_0 + K_w / t} \right) \tag{21}$$

As an example, consider a set of experimental conditions described by Re = 9900 and Pr = 10 in a cell of $r_0 = 1.1$ cm and t = 0.14 cm The physical constants for a pyrex glass wall and the laser liquid $Nd^{+3}:2rCl_4:POCl_3$ are given in Table 1. For the case $T_{CL} - T_0 = 10°C$, we find $T_w - T_0 = 7.7°C$; the bulk of the temperature drop occurs across the cell wall. With this value of T_w, one can obtain the solutions for

$$\frac{T_{CL} - T}{T_{CL} - T_w}$$

TABLE 1

PHYSICAL CONSTANTS OF LASER LIQUID AND LASER CELL

Thermal conductivity of pyrex (K_{pyrex}):	2.7×10^{3} cal • cm^{-1} • s^{-1} • $°C^{-1}$
Density of laser liquid (ρ_L):	1.8 g • cm^{-3}
Index of refraction of liquid ($\lambda = 1.06\mu$, $T = 20°C$) n_0:	1.4783
Change of index with temperature $\left(\frac{dn}{dT}\right)$:	-4.5×10^{-4} $°C^{-1}$
Specific heat of liquid (C_p):	0.320 cal • gm^{-1} • $°C^{-1}$
Prandtl Number of laser liquid (Pr):	10
Dynamic viscosity (μ):	5 centipoise = 5×10^{-2} gm • s^{-1} • cm^{-1}
Thermal conductivity of liquid $\left(K_{liquid} = \frac{C_p \mu}{Pr}\right)$:	1.6×10^{-3} cal • cm^{-1} • s^{-1} • $°C^{-1}$
$T_{CL} - T_0$:	10°C
$T_{CL} - T_w$:	2.3°C

as given by Eqs. (12) to (15). For the conditions specified in the above example, this function:

$$\frac{T_{CL} - T}{T_{CL} - T_w} = 1 - \frac{T_w - T}{T_w - T_{CL}}$$

is plotted against the radius r in Figure 3. The radii r_2 and r_1 shown on the graph are the respective boundaries of the buffer sublayer and laminar sublayers. Also drawn to scale on this figure is the actual laser cell wall thickness t. It is important to note that of the total 2.3°C temperature change between the centerline and the wall less than 7% (0.16°C) occurs up to r = 1.0 cm (the onset of the buffer layer). Most of the temperature drop occurs in the buffer and laminar layers.

Let us now consider the temperature gradient n′(r), Eq. (22):

$$\frac{dn}{dr} = \frac{dn}{dT}\frac{dT}{dr} \qquad (22)$$

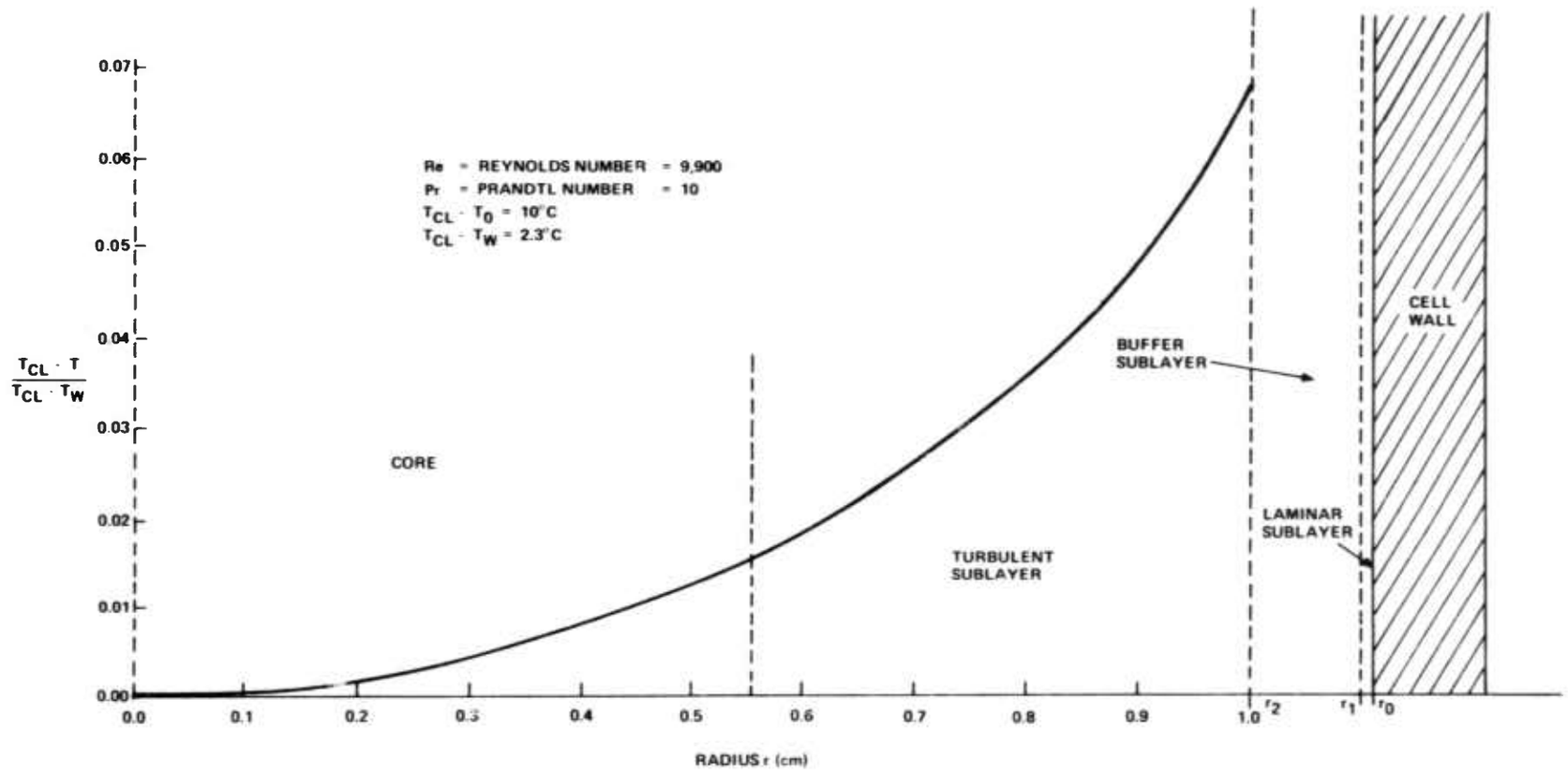

Figure 3. Computer Calculation of Temperature Profile Across the Laser Cell. Parameters are Re = 9,900, Pr = 10. $T_{CL} - T_0 = 10°C$, cell wall thickness = 0.14 cm. The cell wall thickness as well as the four liquid sublayer thicknesses are drawn to scale.

is readily integrated to give:

$$n(r) - n(0) = \frac{dn}{dT}\int^{r} \frac{dT}{dr}\,dr = \frac{dn}{dt}\left(T_r - T_{CL}\right) \tag{23}$$

if we assume $\frac{dn}{dT}$ is constant. Limiting ourselves to the turbulent layer and core and using Eqs. (14) and (15), it is then readily shown that:

$$n(0) - n(r) = \frac{dn}{dT}\left(T_{CL} - T_w\right)\left[1 - \frac{\text{Pr} + \ell n\,[1+5\,\text{Pr}] + 0.5\,\ell n\left[\frac{\text{Re}}{30}\sqrt{\frac{f}{8}}\left(1 - \frac{r}{r_0}\right)\right]}{D}\right] \tag{24}$$

$$\text{for } r_2 \le r \le \frac{r_0}{2}$$

$$n(0) - n(r) = \frac{dn}{dT}\left(T_{CL} - T_w\right)\left[1 - \frac{\text{Pr} + \ell n\,[1+5\,\text{Pr}] + 0.5\,\ell n\,\frac{\text{Re}}{60}\sqrt{\frac{f}{8}} + \left[0.25 - \left(\frac{r}{r_0}\right)\right]^2}{D}\right] \tag{25}$$

$$\text{for } \frac{r_0}{2} \le r \le r_0$$

where D is the same quantity defined in Eqs. (12) to (15). By straightforward differentiation,

$$n'(r) = \frac{dn}{dr} = \left(\frac{-dn}{dT}\right)\left(T_{CL} - T_w\right)\frac{1}{r_0 \times D}\left(\frac{0.5}{1 - r/r_0}\right) \qquad r_2 \le r \le \frac{r_0}{2} \tag{26}$$

$$n'(r) = \left(\frac{-dn}{dT}\right)\left(T_{CL} - T_w\right)\frac{2}{r_0 \times D}\,\frac{r}{r_0} \qquad \frac{r_0}{2} \le r \le r_0 \tag{27}$$

Equation (24) describes the radial variation of the refractive index as a function of the material and flow characteristics and the imposed temperature differential, $T_{CL} - T_0$, since $T_w - T_0$ can be calculated according to Eq. (21). Further, Eqs. (26) and (27) express directly the radial refractive index gradient. Equations (26) and (27) will be applied in the next section to obtain the optical properties of the laser medium.

3.2 OPTICAL CHARACTERISTICS OF THE LASER MEDIUM

For condensed phase lasers, thermo-optical effects arise from the optical excitation energy degraded as heat. In an Nd^{+3} based laser whose principal absorption bands are at 5800 Å and with a laser emission at 1.06 μ, about 45% of the absorbed pump energy is dissipated as heat. For solid state devices there are, in addition, stress-optic effects which complicate the problem. These do not exist in a fluid medium which is subject only to thermo-optical effects.

Thermo-optical effects are of two sorts. The first occurs during the excitation pulse and arises from nonuniform absorption of pump power. This occurs very rapidly in a time of the order of microseconds and the distortion introduced by this process is present for each pulse in a train. The bulk of the excited liquid and the associated heat are swept away after the pulse. However, there is a residue in the laminar and buffer layers which is not exchanged as rapidly as the turbulent core and this gives rise to the second effect. The second effect then occurs on the repetitive application of pulsed energy and is a function of average power. The thermal residues of successive pulses accumulate until the temperature gradient and resulting heat conduction are large enough to balance the increment from each pulse. The radial temperature gradient gives rise to a radial refractive index gradient that distorts the beam in the amplifying medium and results in a marked reduction of output.

In this section we will be concerned with a particular case of the second effect. We will set up a radial thermal gradient through control of T_0 and T_{CL}, $(T_{CL} > T_0)$ the external cell coolant and the bulk temperature of the liquid laser material. As has been shown in the previous section, under these conditions the radial thermal gradient can be evaluated and given this thermal gradient, the refractive index gradient and its effect on the propagated wave will be evaluated. The actual application to laser experiments will be considered later.

A light ray entering normally at the centerline of the laser cell will propagate undeviated. Rays entering normally at values of $r \neq 0$ will deviate from the normal. In fact, since dn/dT and dT/dr have the same sign, the liquid medium will behave as a diverging lens. This is schematically illustrated in Figure 4. The analysis we will give, based on this figure, is taken from Riedel and Baldwin;[7,8] other approaches have been given by Quelle[9] and Winston and Gudmundson.[10]

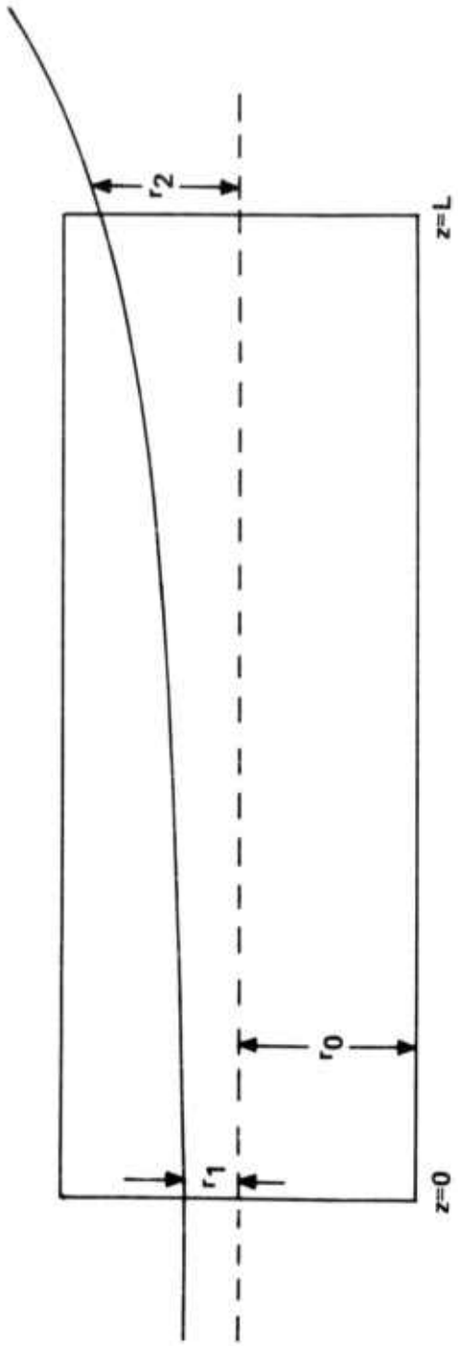

Figure 4. Simplified Ray Diagram of the Laser Cell.

The optical path length, S, of a ray entering at $z = 0$, $r = r_1$, and leaving at $z = L$, $r = r_2$, is given by:

$$S = \int_0^L n(r) \sqrt{1 + n'^2}\, dz = \int_0^L G\,(r, r', z)\, dz \tag{28}$$

where $r' = \frac{dr}{dz}$. Applying Fermat's principle, $\delta S = 0$ leads to the differential equation:

$$\frac{\partial G}{\partial r} - \frac{d}{dz} \frac{\partial G}{\partial r'} = 0$$

$$\frac{dn(r)}{dr} \left(1 + r'^2\right) - nr'' = 0 \tag{29}$$

If we let $q = r'$ and integrate the resulting equation, we find:

$$\frac{1}{2\left(1+q^2\right)} = \ell n\, C_1\, n(r) \tag{30}$$

where C_1 is a constant of integration. This is evaluated by the boundary condition $q\left(r_1\right) = r_1' = 0$. Then

$$C_1 = \frac{1}{n\left(r_1\right) e^{1/2}}$$

and

$$-\frac{1}{2\left(1+q^2\right)} = \ell n \frac{n(r)}{n\left(r_1\right) e^{1/2}} \tag{31}$$

Equation (31) can now be brought into the form:

$$\pm \int \left[\frac{1}{2\ \ell n \frac{n(r)}{n\left(r_1\right)}} - 1\right]^{1/2} dr = \int dz = z + C_2 \tag{32}$$

In the turbulent core, where $\frac{dT}{dr}$ is slowly varying, we express n(r) as follows:

$$n(r) = n_0 + \frac{dn}{dt} \left(T(r) - T_{CL}\right) \tag{33}$$

and using Eqs. (24) and (25),

$$n(r) = n(r_1) + \left(\frac{dn}{dT}\right)\left(\frac{0.5\,(T_{CL} - T_w)}{D}\right) \ell n\left[\frac{R_e}{30}\sqrt{\frac{f}{8}}\left(\frac{r_0 - r}{r_0 - r_1}\right)\right] \tag{34}$$

$$r_2 \leq r,\ r_1 \leq \frac{r_0}{2}$$

$$n(r) = n(r_1) + \left(\frac{dn}{dT}\right)\left(\frac{T_{CL} - T_w}{D}\right)\left[\left(\frac{r_1}{r_0}\right)^2 - \left(\frac{r}{r_0}\right)^2\right] \tag{35}$$

$$\frac{r_0}{2} \leq r,\ r_1 \leq r_0$$

Both expressions may be written in the form:

$$\frac{n(r)}{n(r_1)} = 1 + \frac{C_0}{n(r_1)}\,F(r, r_1)$$

where

$$|C_0| = \left(\frac{dn}{dT}\right)\left(\frac{T_{CL} - T_w}{D}\right) \simeq 10^{-5}$$

$$|F(r, r_1)| \simeq \left(\frac{r_0}{r}\right)^2$$

The insertion of either Eqs. (34) or (35) into Eq. (32) leads to an equation that is not readily integrable.

Over the turbulent iayer and core, $\frac{n(r)}{n(r_1)}$ is a slowly varying function, and can be expanded in a Taylor series:

$$\frac{n(r)}{n(r_1)} = 1 + \frac{n'(r_1)}{n(r_1)}(r - r_1) + \frac{n''(r_1)}{2n(r_1)} + (r - r_1)^2 + \ldots . \tag{36}$$

If we limit ourselves to only the first terms, the expansion of $e^{-a(r - r_1)}$ with $a = \frac{n'(r_1)}{n(r_1)}$ has the same form as Eq. (36). The justification for using this approximation lies in the value of $n'(r_1)$. In general, over the turbulent layer and core, as we have seen, the radial change in temperature is small ($0.16°C$ for $T_{CL} - T_0 = 10°C$). Furthermore, dn/dT is very small, hence $\frac{n'(r_1)}{n(r_1)}$ is very small. Again, over the turbulent layer and core the curvature of T as a function of r is small and $n''(r_1)$ is also small.

From Eqs. (26) and (27) we find, using the first order approximation $n(r_1) \simeq n_0$:

$$a = \frac{n'(r_1)}{n(r_1)} \simeq \left(\frac{-dn}{dT}\right)\left(\frac{T_{CL} - T_w}{n_0 \times r_0}\right)\left(\frac{1}{D}\right)\left(\frac{0.5}{1 - r_1/r_0}\right) \tag{37}$$

in the turbulent layer and

$$a = \frac{n'(r_1)}{n(r_1)} = \left(\frac{-dn}{dT}\right)\left(\frac{T_{CL} - T_w}{n_0 \times r_0}\right)\left(\frac{1}{D}\right)\left(\frac{2r}{r_0}\right) \tag{38}$$

in the core.

Substituting $\frac{n(r)}{n(r_1)} \simeq e^{-a(r - r_1)}$ into Eq. (32) and integrating, we find:

$$z + C_2 = \pm \frac{1}{2a}\left\{\sqrt{2a(r - r_1)}\left[1 - 2a(r - r_1)\right]^{1/2} + \sin^{-1}\left[2a(r - r_1)\right]^{1/2}\right\} \tag{39}$$

C_2 is determined from the boundary condition that at $z = 0$, $r = r_1$; this leads to $C_2 = 0$. Then, using the fact that $a \ll 1$, neglecting $2a(r - r_1)$ with respect to 1 and expanding the arcsine function, we obtain:

$$a^2 z^2 = 2a(r - r_1)$$

or

$$r - r_1 = \frac{a}{2} z^2 = 1/2 \frac{n(r_1)}{n(r_1)} z^2 \tag{40}$$

This says that a ray entering the laser cell normally but off the eylinder axis follows a parabolic path and, since $n'(r)$ ehanges faster than $n(r)$, the curvature of the ray is greater the further it is removed from the eenterline.

3.3 BEAM PROPAGATION IN THE TURBULENT LASER MEDIUM

The parabolic relationship derived in the previous seetion for the ray path has two important eonsequenees. First, a ray entering the medium at ($z = 0$, $r \neq 0$) leaves the medium ($z = L$) at some angle > 0 with respect to the z axis. Secondly, due to the curvature of the ray path there is a phase variation aeross the beam in a plane normal to the propagation direetion after a traversal of the medium. In this section we consider these two factors in more detail.

From the laser cell schematie of Figure 5, the definitions of the quantities shown therein and Snell's law, we can write for the emerging ray:

$$n(r_2) \sin \gamma(r_2) = \sin \varphi(r_2) \tag{41}$$

At r_2,

$$\frac{dr}{dz} = \tan \gamma(r_2)$$

From Eq. (40), we find:

$$\frac{dr}{dz}\Big|_{r_2} = \frac{n'(r_1)}{n(r_1)} L = \tan \gamma(r_2)$$

and then:

$$\sin \varphi(r_2) = n(r_2) \sin \left[\tan^{-1} \frac{n'(r_1)}{n(r_1)} L \right]$$

For the system involved $n'(r_1) \ll L$ and $n(r_1)$, so:

$$\tan \gamma(r_2) = \sin \gamma(r_2) = \gamma(r_2)$$

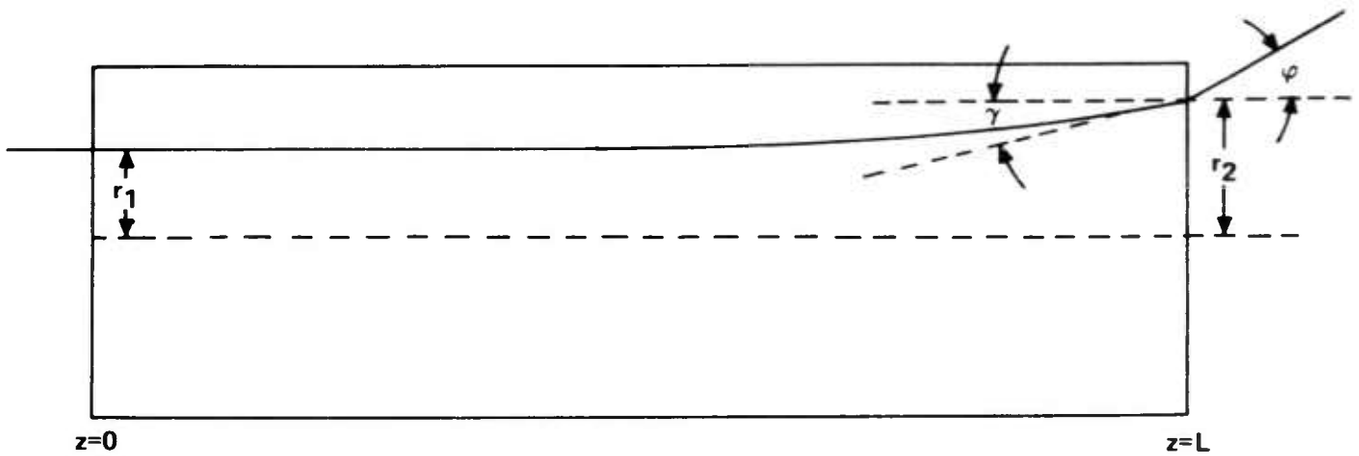

Figure 5. Laser Cell Ray Diagram Showing Ray Exit Angles γ and ω.

then:

$$\sin \varphi\left(r_2\right) = n\left(r_2\right)\frac{n'\left(r_1\right)}{n\left(r_1\right)}L$$

However, since $n\left(r_2\right) \cong n\left(r_1\right)$ and $n'\left(r_1\right)L \ll 1$, then $\varphi\left(r_2\right) = n'\left(r_1\right)L$. The refractive index gradient $n'(r)$ increases with r so that $\varphi\left(r_2\right)$ increases with increasing r_1. At some value of $r_1 = r_a$, the emergence angle $\varphi\left(r_2\right)$ will be large enough so that in a plane parallel resonator, or one with large radius of curvature mirrors, the emerging ray will "walk off" or have a very high loss. From this picture, the laser is then self-apertured at this value of r_a, in general smaller than the turbulent core. The extent of the self-aperturing will depend on the index of refraction gradient and hence on flow conditions and $\Delta T = T_{CL} - T_0$.

With the development of the ray path in the medium, the change in phase along the beam profile can be obtained. This provides an estimate of the beam distortion. Consider the symmetrical arrangement depicted in Figure 6.

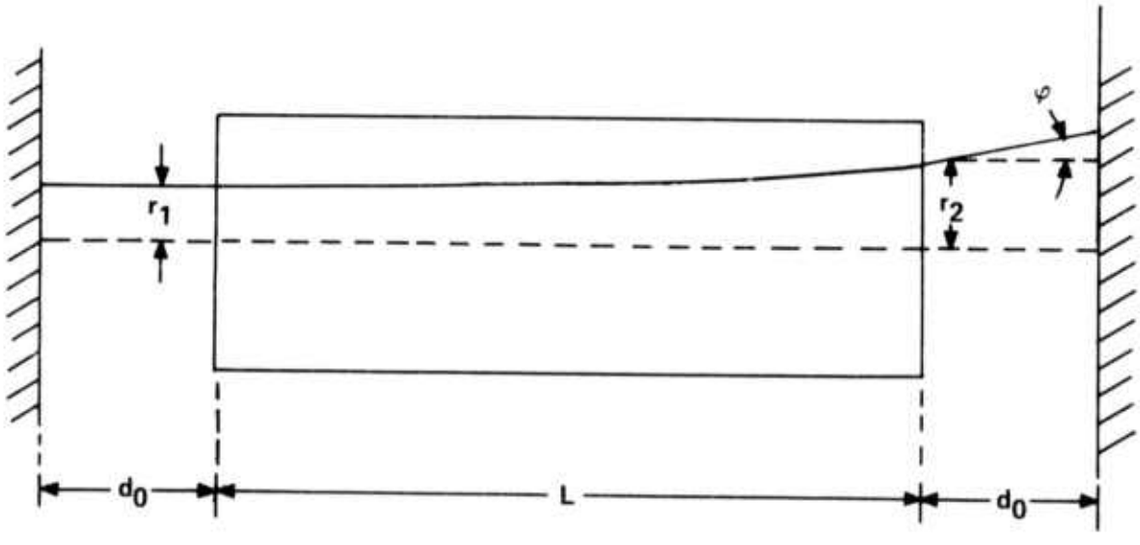

Figure 6. Ray Diagram of the Laser Cell Symmetrically Placed Inside a Plane-Parallel Resonator.

The optical path length of the ray propagated along the centerline is:

$$P(0) = 2d_0 + n_0 L \tag{42}$$

while the general path length is:

$$P(r_1) = S(r_1) + d_0 \left(1 + \frac{1}{\cos \varphi(r_2)}\right) \tag{43}$$

Now,

$$S(r_1) = \int_0^L n(r) \sqrt{1 + r'^2}\, dz \tag{44}$$

and, using Eq. (31), we find

$$S(r_1) = \int_{r_1}^{r_2} \frac{n(r)\, dr}{\sqrt{2\, \ell n \left[n(r)/n(r_1)\right]}} \tag{45}$$

Using Eqs. (36), (40) and the exponential approximation for $\frac{n(r)}{n(r_1)}$, we obtain:

$$S(r_1) = \frac{n(r_1)\sqrt{2}}{a} \int_0^{\frac{aL}{\sqrt{2}}} e^{y^2}\, dy \tag{46}$$

where $y^2 = a(r - r_1)$. Since $y^2 << 1$, we expand the exponential in Eq. (46), retain only the first two terms and integrate to get:

$$S(r_1) = n(r_1)\, L \left\{1 + \frac{a^2 L^2}{6}\right\} \tag{47}$$

then

$$P(r_1) = n(r_1)\, L\left(1 + \frac{a^2 L^2}{6}\right) + d_0 \left(1 + \frac{1}{\cos \varphi(r_2)}\right)$$

Since $\varphi(r_2)$ is small, the cosine can also be expanded to give the final result:

$$P(r_1) = n_0 L + 2 d_0 + \frac{a^2 L^2}{2} \left\{\frac{n(r_1) L}{3} + n(r_1)^2 d_0\right\} \tag{48}$$

Combining Eqs. (42) and (48) and using the definition of a, we find that the change in path length ΔP is:

$$P(r_1) - P_0 = \Delta P = \frac{L^3}{6n_0}\left(1 + \frac{3\,n_0\,d_0}{L}\right)n'(r_1)^2 \tag{49}$$

Actual numerical evaluation of ΔP is considered in Section 5.4.

4. THE LIQUID LASER

Apart from the fact that the active medium of liquid lasers is liquid, the total system is conceptually similar to comparable solid state systems The fluid nature of the active medium presents a set of technological problems and forms the basis for the advantages and disadvantages of the system. Technologically one is faced with the following problems: first, to circulate a chemically reactive liquid which is sensitive to water in a small, closed system while avoiding contamination; second, to design the active laser region so that the optical quality is excellent.

The basic conceptual advantage of the liquid laser is the ability to cope with the thermal problems arising from high average input powers. Heat dissipation is not limited by thermal conductivity since the fluid nature adds a convective capability. In addition, one can control the temperature of the active medium and the external cell wall (the latter is equivalent to the conventional cooling method for solid state devices) separately, and this provides an additional degree of control over radial thermal gradients. The principal disadvantage arises from the large temperature coefficient, dn/dT, of the index of refraction; this tends to magnify small temperature differences from an optical viewpoint. In this section we will discuss the design and construction of the liquid laser, indicating how the technological problems can be brought under control, and how the cooling and power systems interface with the circulatory system.

4.1 CONSTRUCTION AND ASSEMBLY OF THE SYSTEM

The liquid laser system consists of three components: the circulatory system, the power supply, and the cooling system. The latter two are commercially available and will be described later. We will focus our attention on the circulatory system first.

4.1.1 The Circulatory System

The circulatory system is schematically illustrated in Figure 7. In this arrangement, the three cells are in series and a reference pressure surface is located between the two large units. A two-micron porosity cylindrical quartz filter is in a parallel arrangement across the three heads. A constrictive resistance is placed in series with the filter to limit the flow through this path to about 10% of the total volume flow. The components are connected with one-inch diameter Corning beaded glass pipe and Corning couplers. As few couplers as possible, consistent with convenience and

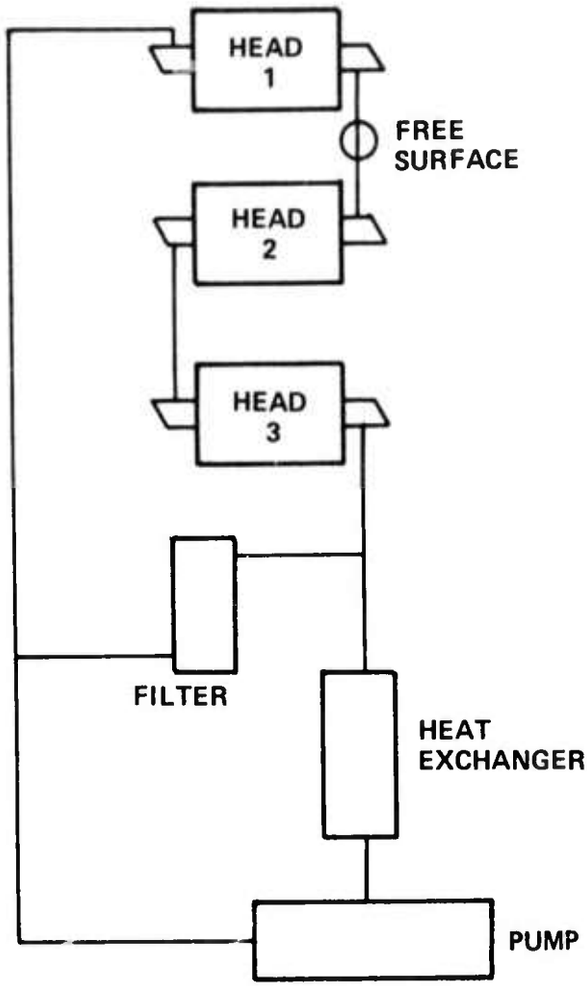

Figure 7. Liquid Laser Circulatory Schematic Diagram.

strength, are used. In addition, the pipe and couplers are sealed externally with RTV as a safety factor. The three features requiring further elaboration are the cell, the pump and the flash enclosures.

The type of cell used is illustrated in Figure 8. The body of the cell is pyrex tubing of the appropriate bore diameter and wall thickness. Sealed to each end of the tube is a truncated conical pyrex end piece having a centrally located hole the same size as the bore diameter of the tube. In actual fabrication, one conical piece is first attached and a water jacket of appropriate dimensions slipped over the unfinished end and then the second conical piece is added. The thick ends of the cell are ground and polished to be flat and parallel. Teflon-covered O-rings are used to seal the finished cell body to nickel plenum chambers at each end. The plenum chambers consist of a nickel tube with an inlet pipe at right angles which is terminated with a bead to mate to the Corning glass pipe. The assembled cell is then completed at each end by a two-inch thick homosil quartz window. The end of the window facing the liquid and the nickel transition piece are both tapered as they approach the cell entrance so that the window diameter matches the cell diameter. The annular space between the window and the nickel transition piece is made to have an area as close as possible to the cell cross section. In this way the velocity of the liquid, on entering the cell, changes in direction only but not in speed.

The volume enclosed by the nickel transition piece acts as a plenum chamber. There is vigorous mixing as the liquid flow enters and is diverted by the nose-piece of the cell window. The flow then assumes a new direction and the liquid enters onto its journey down the cell (pipe). For the three-head arrangement illustrated in Figure 7, the cell geometry and flash head are given in Table 2.

In general the objective is to exchange the liquid in the cell once per pulse. At a maximum of 5 pulses per second this corresponds to a linear speed of about 180 cm/s. For a 2.2-cm diameter cell, the volume flow rate is about 700 cc/s, and, given a density of 1.8 g/cm^3 and a viscosity of 5 centipoise, the Reynolds number of the flow is about 14,000. This is well in the turbulent regime. With the series cell arrangement shown, this flow rate cannot be readily achieved because it results in cavitation. For the largest cell, Reynolds numbers between 6,000 and 10,000 were available but in the smaller cell higher Reynolds numbers could be reached.

Another feature of the cell and water jacket arrangement is the optimization of the coupling of the lamps to the active volume. This, in fact, is related to the problem

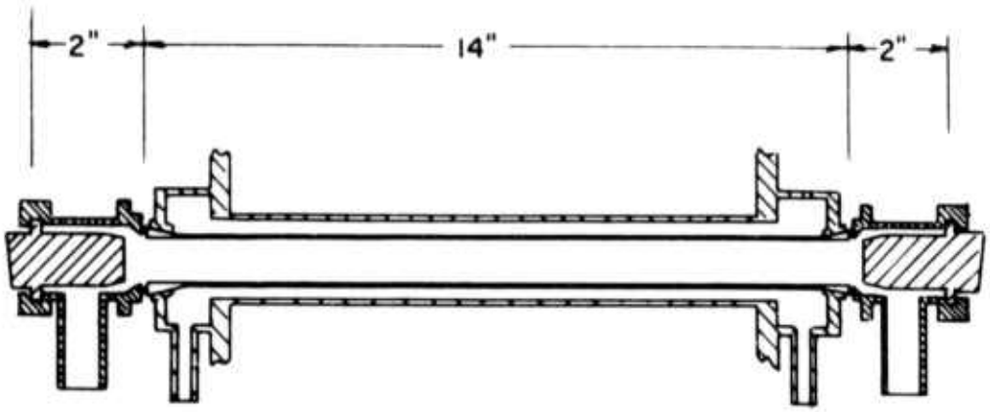

Figure 8. Cutaway View of Actual Water-Jacketed Laser Cell Demonstrating Cell Assembly.

TABLE 2

CELL DIMENSIONS AND FLASH HEADS FOR LIQUID LASER SYSTEM

Item	Head #1	Head #2	Head #3
Flash Enclosure	Quad Ellipse	Dual Ellipse	Dual Ellipse
Number of Lamps	4	2	2
Pumped Cell Length	10 inches	10 inches	6-1/2 inches
Cell Bore Diameter	7/8-inch (2.2 cm)	5/8-inch (1.6 cm)	1/2-inch (1.3 cm)
Cell Active Volume	100 cm^3	50 cm^3	20 cm^3
E_{input}/pulse (maximum)	4000 joules	2000 joules	750 joules
Maximum Rep. Rate	5 pps	10 pps	20 pps
Laser Cell Wall Thickness	0.14 cm	0.10 cm	0.08 cm
Thickness of Water Coolant Layer	0.31 cm	0.20 cm	0.14 cm
Glass Water Jacket Thickness	0.10 cm	0.10 cm	0.10 cm
O.D. of Glass Water Jacket	3.32 cm	2.40 cm	1.90 cm

of a sheathed laser rod[11, 12] and the analysis follows the diagram in Figure 9. The basic idea is to design the cell wall thickness, the cooling jacket and its wall thickness so that a pump ray tangential to the external wall of the water jacket is also tangential to the internal wall of the cell. The figure shows a tangential light ray entering the assembly at point M. This ray is refracted by the water jacket assembly to strike the laser cell tangentially at point 0. The laser cell wall thickness, $r-\rho$, is chosen such that the ray then strikes the laser liquid tangentially at point P. The latter condition is assured by the relation:

$$n_2 r = n_1 \rho; \quad r = \frac{n_1}{n_2}\rho \tag{50}$$

Referring to the figure, we have for the incident ray at point M,

$$\begin{aligned} n_1 \sin\theta_1 &= \sin(\pi/2) \\ \sin\theta_1 &= 1/n_1 \end{aligned} \tag{51}$$

and at point N,

$$\sin\theta_2 = \frac{R \sin\theta_1}{R-t} = \left(1/n_1\right)\frac{R}{R-t} \tag{52}$$

Then, from Snell's Law,

$$\sin\theta_3 = \left(1/n_2\right)\frac{R}{R-t} \tag{53}$$

In addition,

$$\frac{r}{\sin\theta_3} = \frac{R-t}{\sin(\pi/2)} = R-t$$

Thus,

$$\begin{aligned} \sin\theta_3 &= \frac{r}{R-t} = \frac{R}{n_2}\left(\frac{1}{R-t}\right) \\ r &= R/n_2 \end{aligned} \tag{54}$$

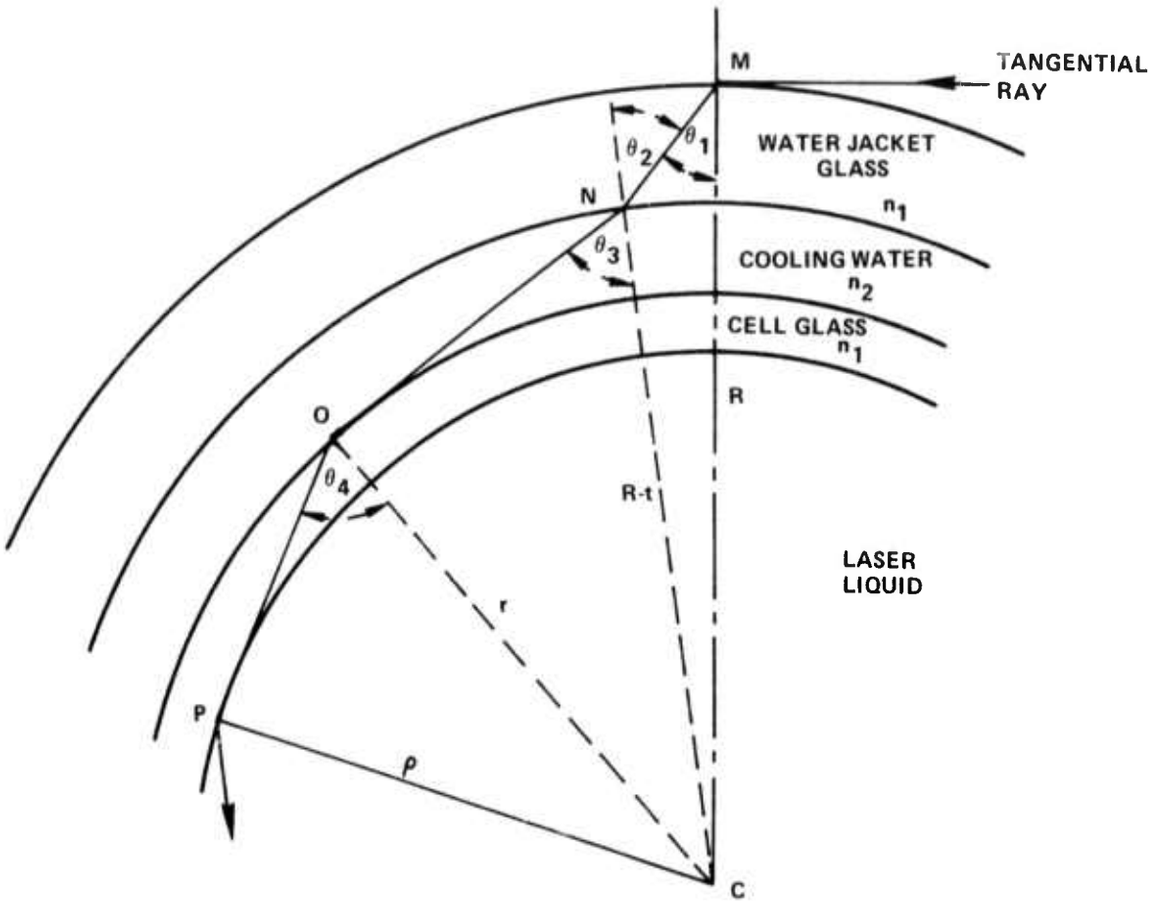

Figure 9. Ray Tracing Diagram for Calculating Optimum Coupling of Flashlamp Radiation to the Laser Liquid.

We must impose the constraint at the point N that the angle of incidence θ_2 does not lead to total reflection, i.e.,

$$\sin\theta_3 \leq 1 \tag{55}$$

Using Eq. (9), we have

$$\frac{R}{n_2}\left(\frac{1}{R-t}\right) \leq 1$$

$$R \leq n_2 (R-t)$$

$$t \leq R\left(1 - \frac{1}{n_2}\right) \tag{56}$$

Equations (50), (54), and (56) serve to define the design constraints given a desired cell bore radius, ρ, and cell and water-jacket material (pyrex, $n_1 = 1.45$) with water ($n_2 = 1.33$) as the cell collant. The dimensions are listed in Table 2.

The circulatory pump is a critical element since the purity of the liquid depends on how well it performs, and it is clear that almost any direct means for transmitting the driving power to the pump creates a shaft-seal problem both in terms of packing material and atmospheric leakage. The best and thus far only long-lived solution to this problem was found in a "canned" pump manufactured by the Liquid Dynamics Corporation.

The pump itself is schematically illustrated in Figure 10. The driving power is electromagnetically transmitted from a rotating field to a soft iron core encapsulated in a nickel case. The impeller, pump casing and rotor housing are all fabricated from Carpenter 20 stainless steel, and the bushings, journals and associated locating hardware in contact with the liquid are either alumina or stainless steel. In the pump, as well as in the rest of the system, the liquid comes into contact only with the materials mentioned toward which it is nonreactive or with which it reacts exceedingly slowly as determined by corrosion tests.[13] The pump has been operated above and below atmospheric pressure and has proven to be reliable and tight with respect to leaks. The characteristics of the pump are illustrated in Figure 11.

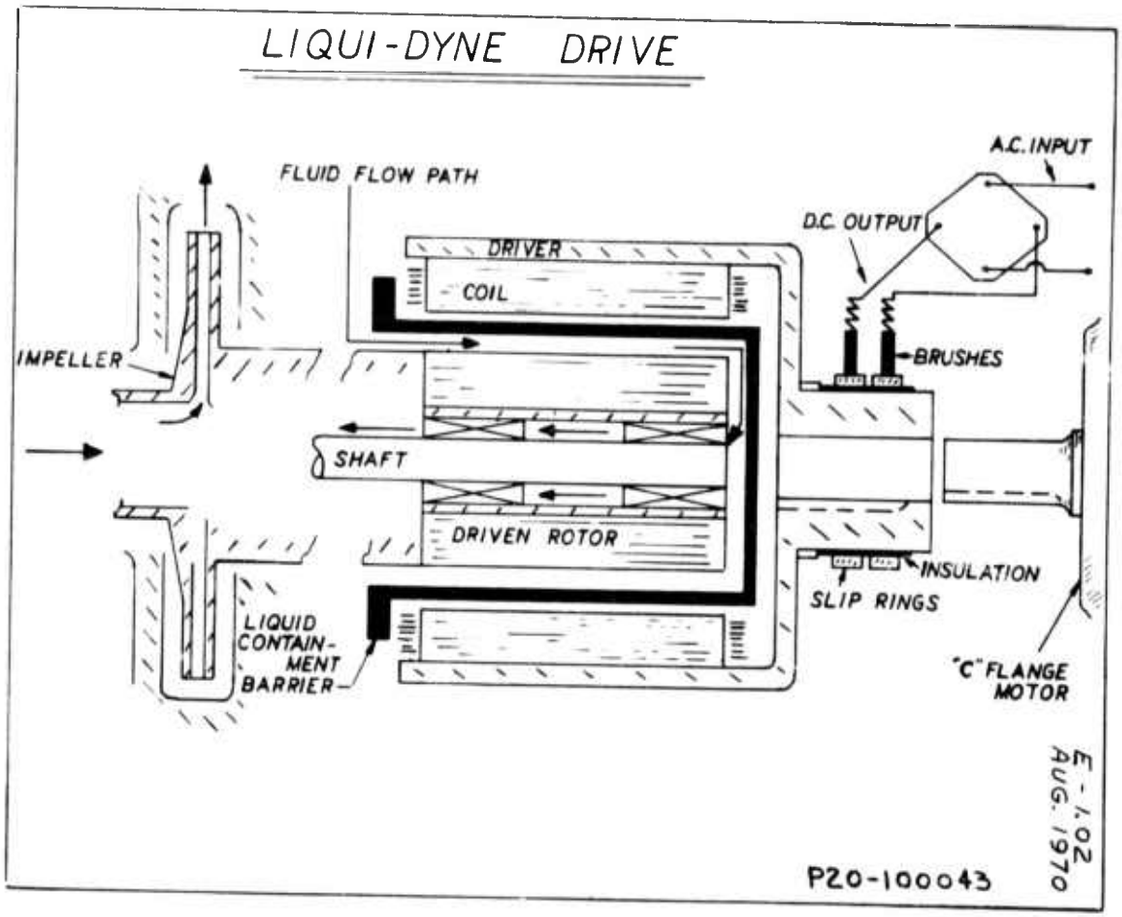

Figure 10. Cross-Section of Circulating Pump Manufactured by Liquid Dynamics, Inc.

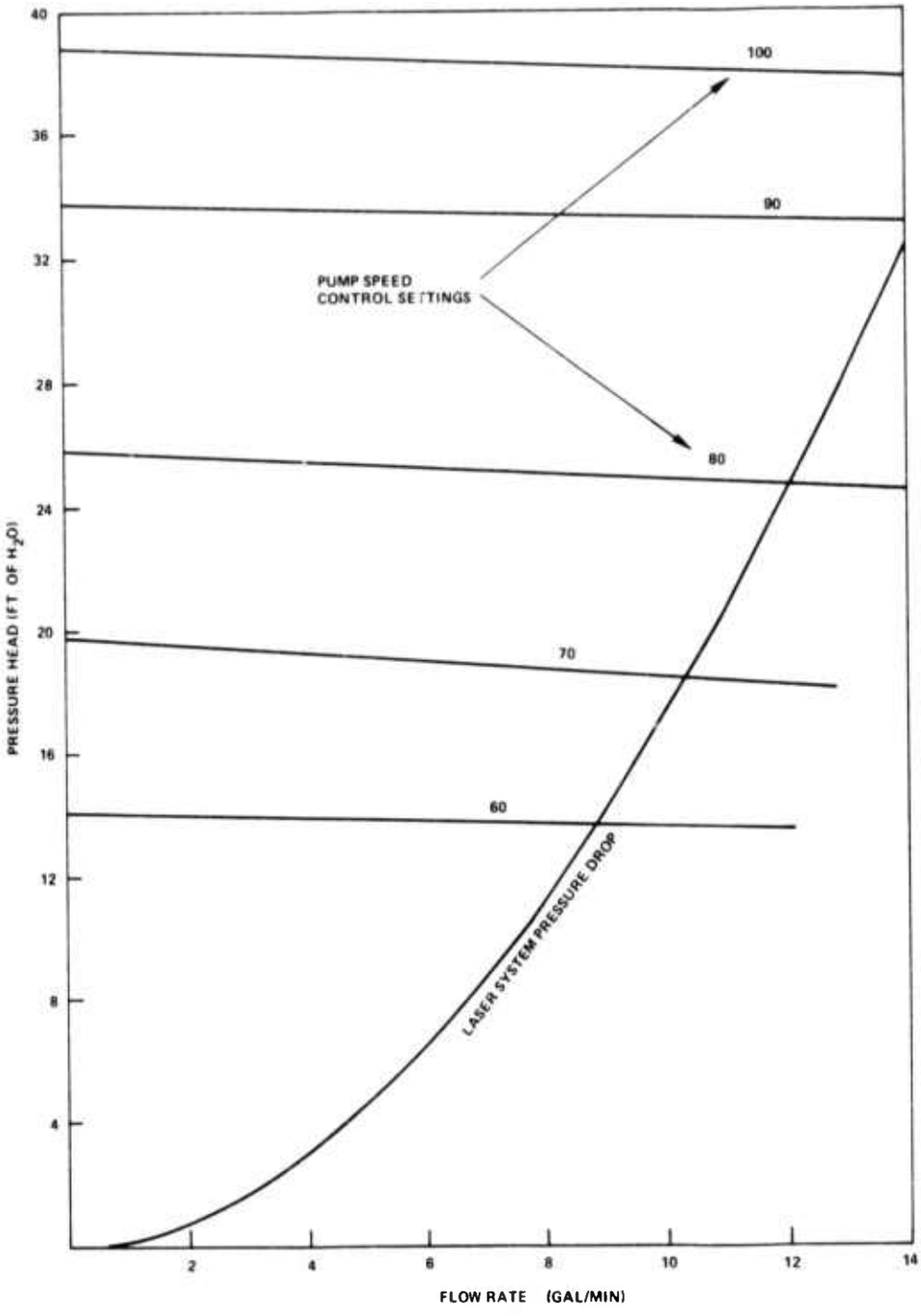

Figure 11. Pressure-Flow Rate Characteristic of the Laser System Using the Liquid Dynamics Pump.

Also, in the circulatory system are a heat exchanger, a liquid filter and a free surface. The heat exchanger is of the shell and tube type with water as the coolant. All the tubes and the end volumes are made from high purity nickel for chemical compatibility. The use of nickel limits the efficiency of the heat exchanger, and it proves to be a marginal component in this system. The filter is a 2-μ porosity cylindrical fritted quartz element in a parallel arrangement with the cells. Flow through the filter loop is controlled by a constriction in the tubing.

The free surface is connected to a 5-liter gas ballast and, through this by means of a three-way stopcock, to a mercury bubbler or a source of dry nitrogen. This is the only contact the laser liquid has with the outside world and it plays an important role in filling the system, in degassing the laser liquid, and in pressurizing the system. It also, to some extent, functions as a shock absorber for the thermal shock occurring when the laser is pulsed.

After the system is assembled, the strain in the assembly is relieved by heating the glass pipe at points of stress. The system is checked for tightness by pressurizing to about 1 atmosphere and checking for leaks. When this is found to be satisfactory, the drying and filling procedure is undertaken. The circulatory system is filled with dry $POCl_3$ (< 5 ppm) which is then circulated for several days during which time samples of the solvent are withdrawn periodically and analyzed for their water content. A given fill of $POCl_3$ is retained in the system until its water level remains relatively constant for several days or it becomes excessive (>150 ppm). The $POCl_3$ is then drained and replaced with a new, dry quantity. This rinsing procedure is continued until the steady water level of the $POCl_3$ in the system is reduced to 10 ppm or less. Then, after this is drained, the system is filled with the laser solution.

Several techniques have been used to carry out the final filling. The one that has proved most convenient is to fill the system by forcing the laser liquid in by pressure through the petcock located at the bottom of the pump. After the liquid has been filled to the level of the ball in the free surface, the pressure at the free surface is slowly and carefully reduced by pumping with a mechanical pump through the three-way stopcock and the gas ballast. This is done in stages and at each stage the circulatory pump is turned slowly and the trapped gas is evolved. This procedure is continued until the free surface pressure is reduced to about 1/2 atmosphere and there is very little evolution of gas with the circulatory pump running at speeds to be used in later experiments. This procedure ensures that there are no trapped gas pockets in the circulatory

system and that a good part of the gas dissolved in the laser liquid has been removed. Unless this procedure is carefully carried out these residual gases will evolve as a stream of fine bubbles and result in significant losses during laser operations. These fine bubbles will be only slowly removed since, on circulation, only a few will rise to the free surface; most tend to remain in the main stream.

4.2 THE POWER SUPPLY AND COOLING SYSTEM

The mode of operation of the liquid laser being described here is pulsed. The power supply must be capable of producing high energy pulses at repetition rates up to 10 pps. The one we have used is the M-60 power supply manufactured by Systomation, Inc. This unit can deliver an average power of 30 kW to the capacitor banks but, because of flash lamp limitations, we have rarely exceeded 20 kW.

The energy is stored in a simple pulse forming network illustrated in Figure 12. For the four-lamp enclosure, the lamps are divided into two sets in parallel and within a set, two lamps are used in series. Each set is energized by its own set of capacitors. For the large two-lamp enclosure only one part of the bank is used and for the small two-lamp enclosure the pulse forming network is modified as shown in Figure 13.

The cooling system is a modification of the unit manufactured by Systomation, Inc. One Harrel temperature regulator controls a water-to-water heat exchanger. This is a closed loop filled with demineralized water and is used for the flash lamps and the water jacket on the laser cell. It has the capacity to handle the 20 kW input power. A second Harrel temperature controller is used for the laser liquid heat exchanger. This is a demand unit and allows water from the municipal supply to flow through the heat exchanger. The sensors activating the controllers are plantinum resistance thermometers, one located on the glass pipe feeding the laser liquid into the largest cell and the other internal to the demineralized water loop. To monitor system temperatures, iron-constantan thermocouples, located at the same places as the sensors, are used.

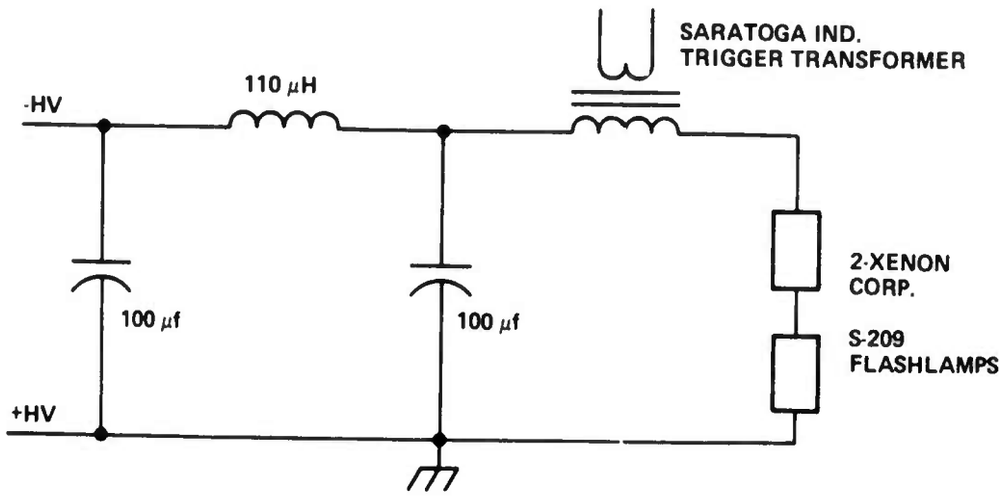

Figure 12. Pulse Forming Network for Two Largest Laser Heads.

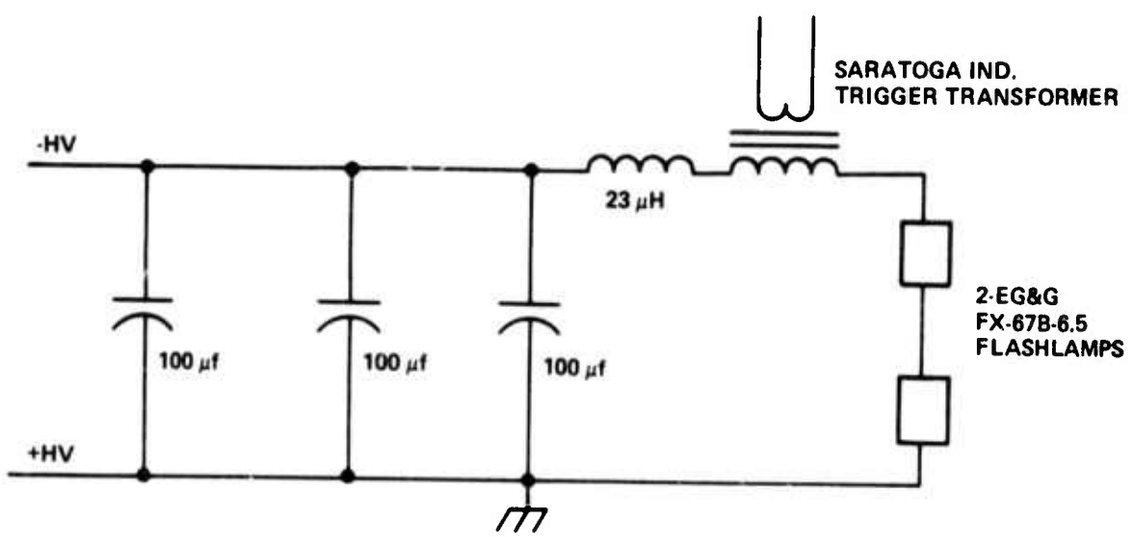

Figure 13. Pulse Forming Network for Smallest Laser Head.

5. EXPERIMENTAL RESULTS

The circulability of the active medium in a liquid laser makes it possible to present a new isothermal liquid sample for each flashlamp pulse. In view of this, the most natural mode of operation would be that of repetitive pulsing in the high average power range. However, the inevitable existenee of a laminar layer (a virtually stagnant layer immediately adjacent to the cell wall) and the faet that the eell wall itself absorbs radiation leads to a residual thermal problem. The purpose of the external eell cooling is to provide a measure of eontrol over this remaining problem.

Coneeptually, the objective in the design of the system is to achieve, as nearly as possible, an isothermal, optically homogeneous gain medium for each pulse. The degree to which this is achieved is measured by how the pulse output under repetitive pulsing compares to the pulse output under single-shot, isothermal conditions. Experimentally we control the temperature of the laser liquid (T_{CL}) and that of the external eoolant (T_0), and ean vary the input pulse energy and the repetition rate (average power loading). For a given set of eonditions we observe the steady-state pulse output energy. To do this, the pulse train must be run long enough so that a steady state has time to develop.

We will first eonsider experiments under isothermal eonditions. This provides a basis for determining the dynamie loss and a referenee pulse output energy. Following this, the results for various temperature differentials, $\Delta T = T_{CL} - T_0$, and varying average input powers will be presented and discussed.

5.1 EXPERIMENTAL ARRANGEMENT

The laser system has been deseribed in Seetion 4. The measurements of output energy were made using a calibrated photo diode (EG&G Lite-Mike) whose output was recorded on a Honeywell Visicorder. The output of the laser was direeted into a beam splitter arrangement shown in Figure 14. The transmission factor of the beam splitter and colleeting lens was measured using a ew YAG laser. The YAG output was measured with an EG&G Radiometer first direetly and then after passage through the beamsplitter-lens combination. This was repeated ten times and the average transmission factor of 0.777 obtained. Calibration of the Lite Mike was then performed as follows. The Radiometer was replaced with a T.R.G. Ballistic Thermopile and the Lite-Mike placed at one of the other output ports. An opal diffusing plate, a neutral density filter (T = 0.116) and a silieon wafer were inserted between the beamsplitter and the Lite-Mike.

Preceding page blank

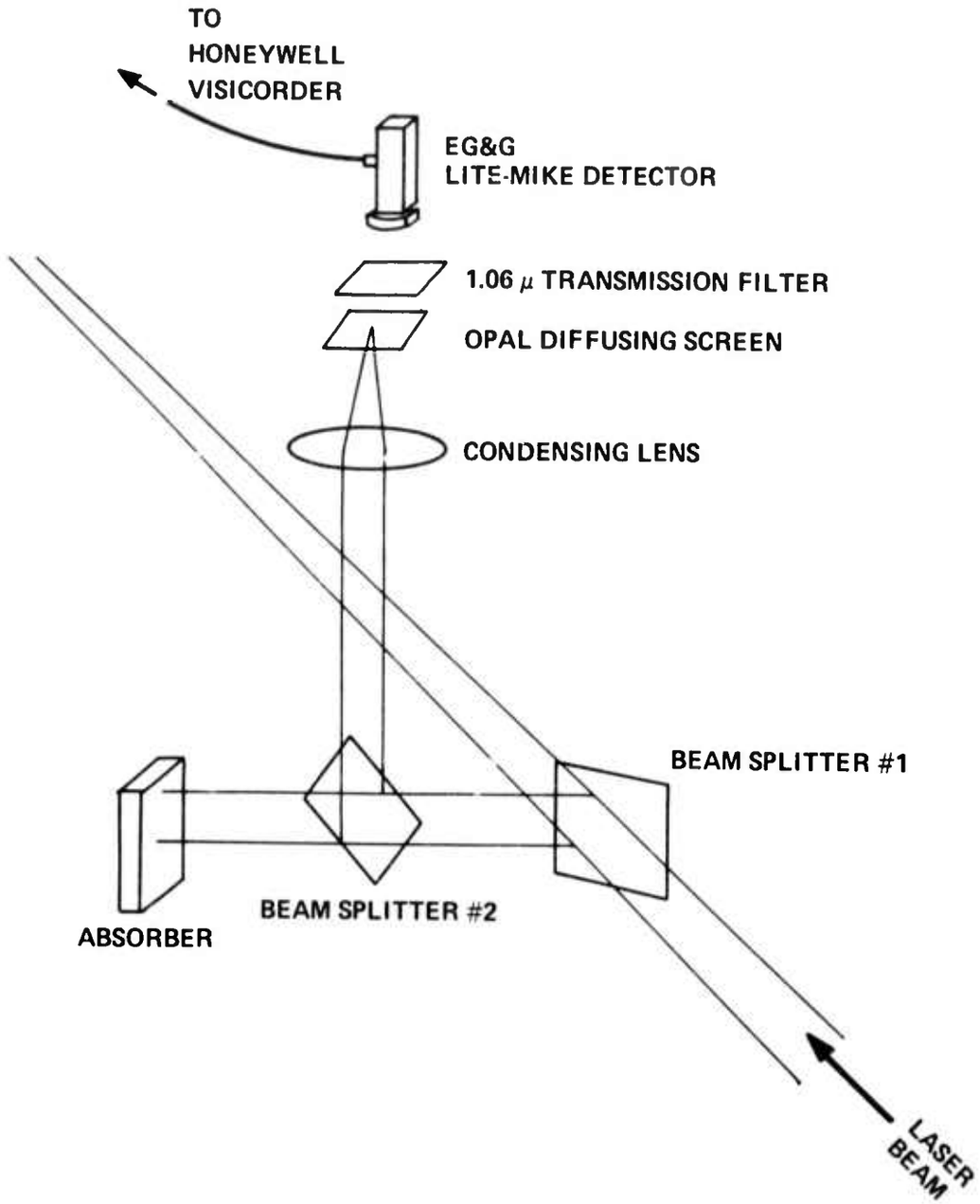

Figure 14. Arrangement for Measuring Output Pulse Energy in the Laser Beam.

The liquid laser was pulsed and a simultaneous record of the thermopile and Lite-Mike (used in the integrating mode) voltages recorded. This procedure was repeated many times at different output levels and the volts per joule value for the detector and beam-splitter combination established.

5.2 EXPERIMENTS UNDER ISOTHERMAL CONDITIONS

The experiments performed under isothermal conditions ($\Delta T = 0$) were carried out in two ways. First, the pulse repetition rate was kept constant at 0.5 pps and 1.0 pps and runs of between 10 and 20 pulses were made at varying input pulse energies. Second, the pulse repetition rate was varied at each input pulse energy level so that the average input power was maintained constant at 250 watts. For each point, a train of between 10 and 20 pulses was run and the average was used as the output. The cavity was formed by two mirrors with each having a radius of curvature of 5 meters; one mirror had a maximum reflectivity nominally 99.8%, while the reflectivity of the other, the output mirror, varied. Five different output reflectivities ranging from 82.7 to 34.5% were used, and the results for the extreme output reflectivities are shown in Figure 15. At the higher power loadings, in the curves illustrated, the output energy for 1 pps is usually greater than that for 0.5 pps. This, however, is not always the case and, in this instance, it could easily be due to a temperature differential $\Delta T = T_{liquid} - T_{coolant}$. Nominally, the two temperatures were equal but, for practical purposes, this means that $|\Delta T| < 0.2^{\circ}C$; in the event $\Delta T > 0$, higher average input power would tend to improve the laser output. It should also be noted that at the higher reflectivity there is a marked curvature at the higher output levels. This characteristic of liquid lasers has been observed before[14] and will not be discussed here. At lower input energies, however, the plots do become linear and a linear extrapolation to a threshold can be made. Experiments with constant input power are consistent with the results for constant repetition rate pulsing and do extrapolate to the same thresholds.

It has been shown[14] that, to a good approximation, the output energy of the laser, E_{out}, is given by the expression:

$$E_{out} = \eta_s^0 (E_{in} - E_{th}) \frac{T}{T + A} \tag{57}$$

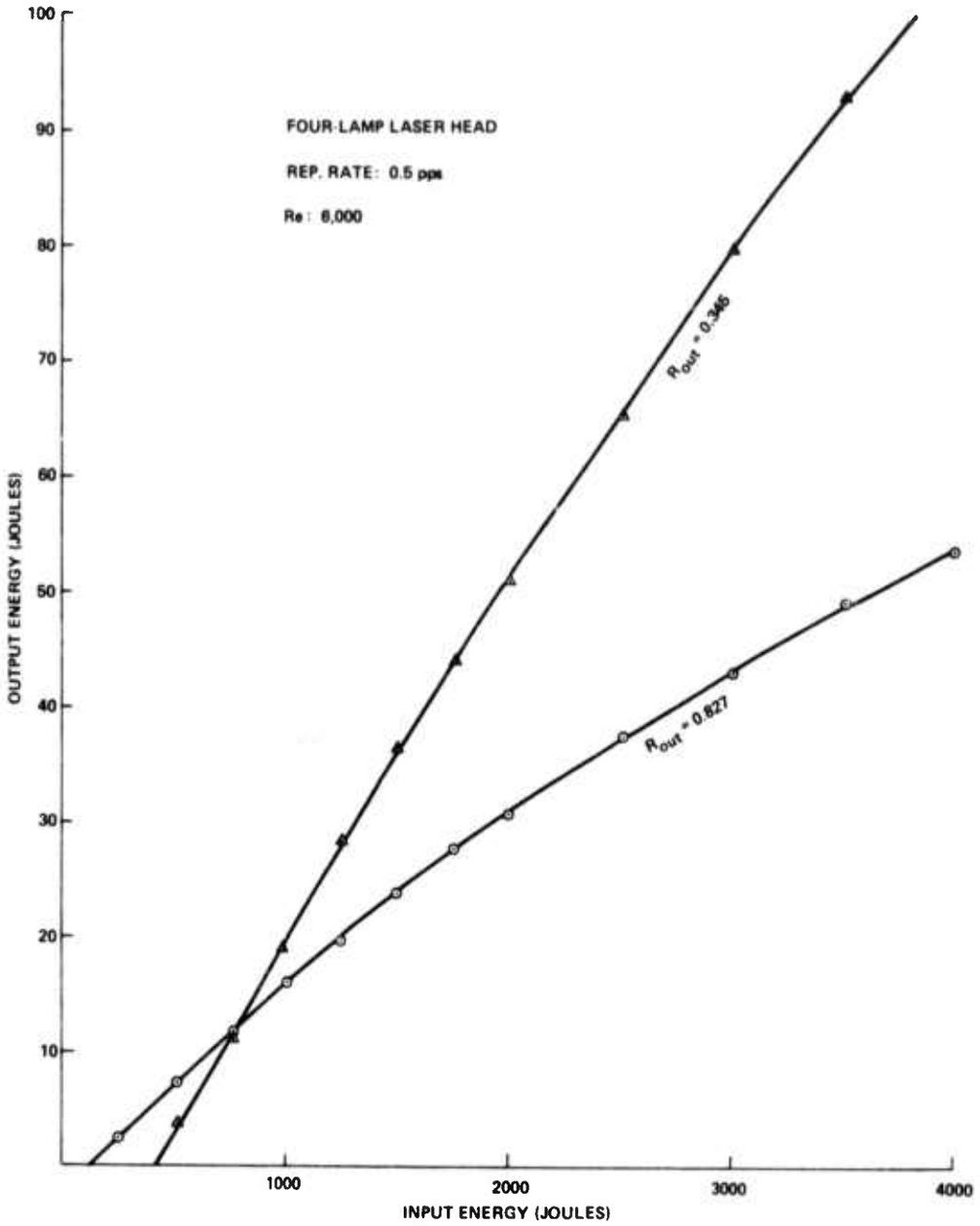

Figure 15. Output Pulse Energy vs. Input Energy for Four-Lamp 10-Inch Laser Head. The two extremes of output mirror reflectivity are shown. Reynolds number: 6,000. Pulse repetition rate: 0.5 pps.

where

η_s = slope efficiency

η_s^0 = slope efficiency at zero output coupling

E_{in} = input energy

E_{th} = threshold energy

T = output mirror transmission

A = distributed losses in the laser medium

The threshold energy,[14] E_{th}, is given by:

$$E_{th} = \frac{\alpha}{\beta\sigma} - \frac{\ell n\, R_{out}}{\beta\sigma L} \qquad (58)$$

where

β = constant involving various efficiency factors, most of which are not well-known

σ = absorption cross section in the laser transition

L = round trip path length in the active medium

$\alpha = A/L$

Only R_{out} appears in this equation since it is assumed that the other cavity mirror has unit reflectivity. Equations (57) and (58) can be used to provide a measure of A or α, the dynamic loss of the active medium. The appropriate plots are shown in Figures 16 and 17, and from these a loss value, α, between 0.3 and 0.5% cm^{-1} is obtained.

The data discussed to this point concerns the quadruple ellipse flash head with a cell having the dimensions of 10 inches in length and 7/8 inch in diameter. Typical results obtained with the other 10-inch double ellipse flash head are shown in Figure 18. In these heads the input energy is limited by the flash lamps. For the smaller head, the threshold energies and slope efficiencies are slightly lower than for the large head. The dynamic loss, a property of the medium itself, falls within the range already established for the four-lamp flash head.

5.3 EXPERIMENTS AT HIGHER PULSE REPETITION RATES

The experiments described in the preceding section can be viewed as single shot in nature. The repetition rate is sufficiently low and the flow rate sufficiently fast

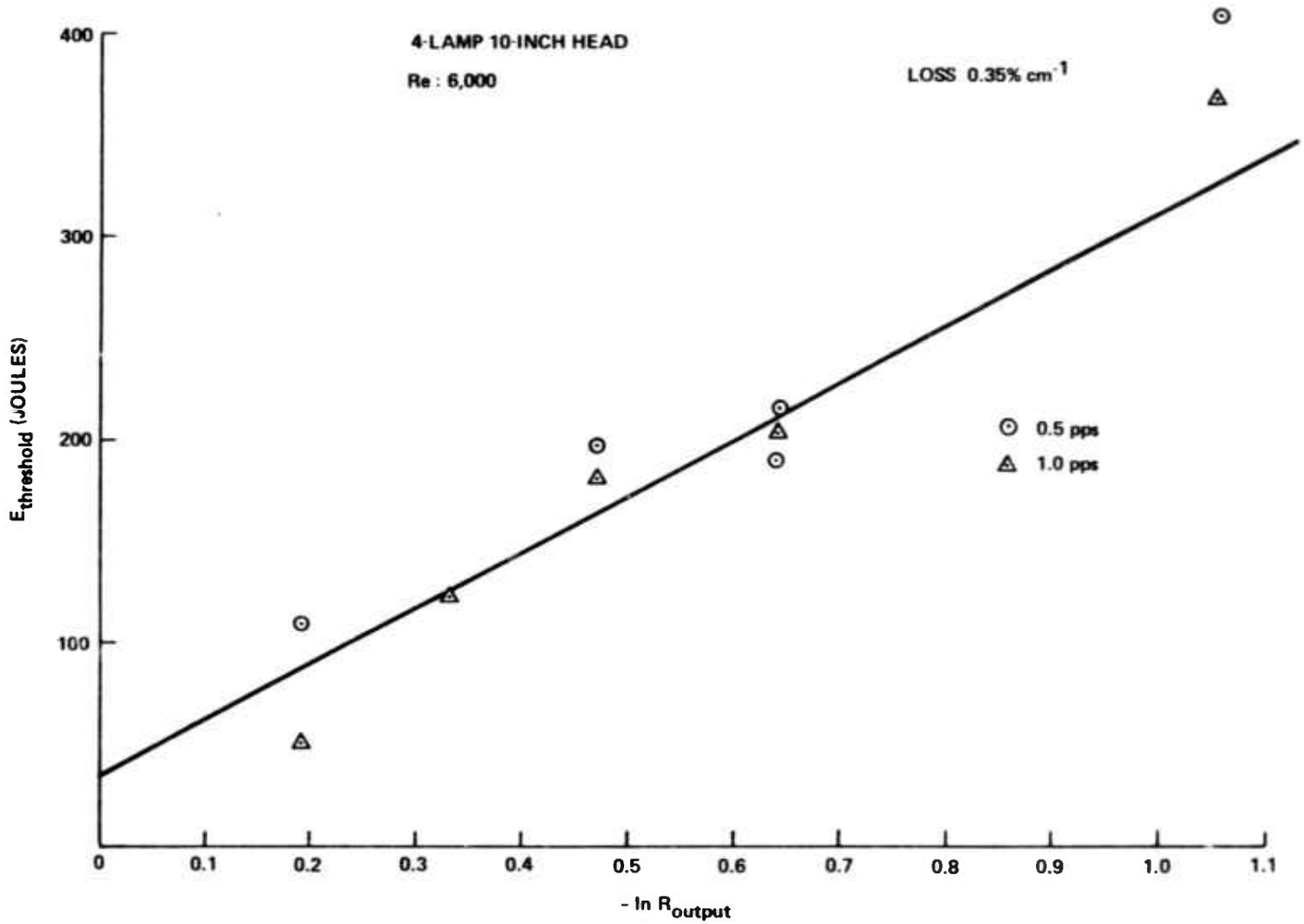

Figure 16. Laser Threshold Energy vs. $-\ell n\ R_{out}$ for Four-Lamp 10-Inch Head. Pulse repetition rates: 0.5 and 1.0 pps. Data indicates distributed loss of 0.35% cm^{-1}.

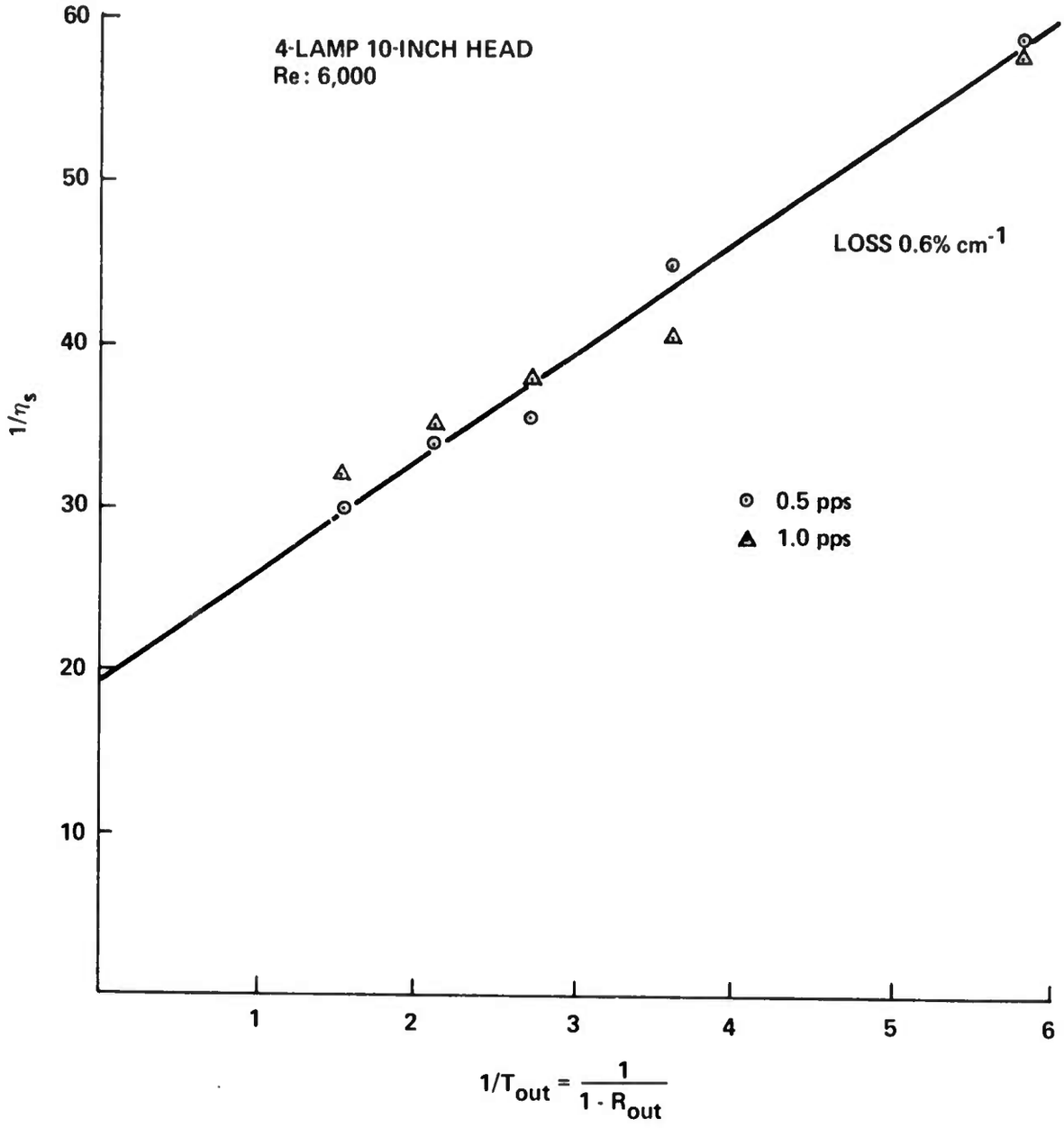

Figure 17. Reciprocal of Laser Slope Efficiency vs. $1/1\text{-}R_{out}$ for Four-Lamp 10-Inch Head. Reynolds number: 6,000. Pulse repetition rates: 0.5 and 1.0 pps. Data indicates distributed loss of 0.6% cm^{-1}.

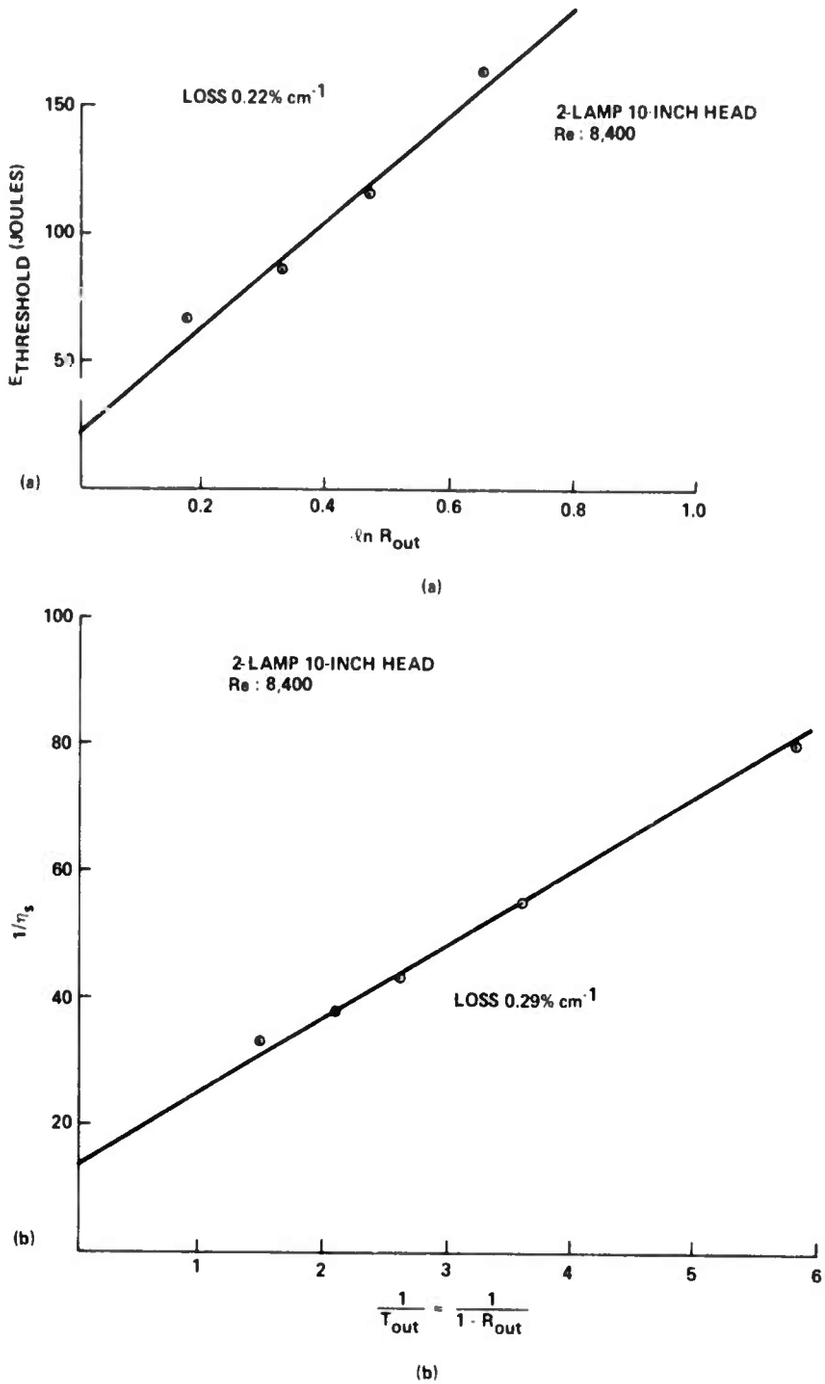

Figure 18. Loss Measurements for Two-Lamp 10-Inch Head. Reynolds number: 8,400. Pulse repetition rate: 0.5 pps.

(a) Laser threshold energy vs. $-\ell n\ R_{out}$. Data indicates loss of 0.22% cm^{-1}.

(b) Reciprocal of laser slope efficiency vs. 1/1-R. Data indicates loss of 0.29% cm^{-1}.

so that the aspect the liquid and cell present to the cavity is the same from shot to shot. The average power output is thus limited by the low repetition rate within the safe operating range of the flash lamps. A more interesting mode of operation is at high average power and this is achieved by increasing the pulse repetition rate. At the higher average input powers, however, there are cumulative thermal effects. The heat dissipated within the cell by one shot is not all removed before the next shot occurs. As a consequence, a radial thermal gradient and a concomitant refractive index gradient develop and the optical quality of the gain medium is drastically reduced.

Such thermal effects are well-known in high average power operation of condensed phase lasers. In general, it manifests itself by a decreasing output energy for each subsequent pulse at constant input pulse energy. In many cases, a steady pulse output energy at a much lower level than the single-shot values is established. To achieve improved high average power performance, it is essential to eliminate, or at least minimize, the effect of the cumulative thermal effect resulting from excitation of the laser. The customary approach is to cool the active medium. In the case of a liquid active medium, it can also be circulated, and this provides considerable assistance in controlling the radial gradient.

In this section we will detail the results of high average power experiments. First, however, we will discuss the way in which the results will be characterized. Since the power loading varies with both pulse input energy and repetition rate, the concept of slope efficiency and extrapolated threshold lose their unique meaning. The most convenient references are the results of the single-shot experiments described in the preceding section. We designate these results by E_0, and they will depend on the input pulse energy and flow speed. In addition, we have to decide upon which pulse or pulses in the train are to be used to characterize the laser. In general, the pulse output energy is variable in the early part of a train and depends on the flow speed, temperature differential and average input power. Some typical pulse trains are illustrated in Figure 19. In all cases, if the pulse train were sufficiently long, a steady output pulse energy would be achieved and this steady value is used to characterize a particular set of laser operating parameters. This value, designated as E (a function of input energy, pulse repetition rate, temperature differential and flow speed) and the ratio E/E_0, is used as the dependent variable. As the independent variable, we use the average input power. It is clear from the experiments described in the preceding section that this is an approximation. For example, a large pulse energy infrequently repeated does not

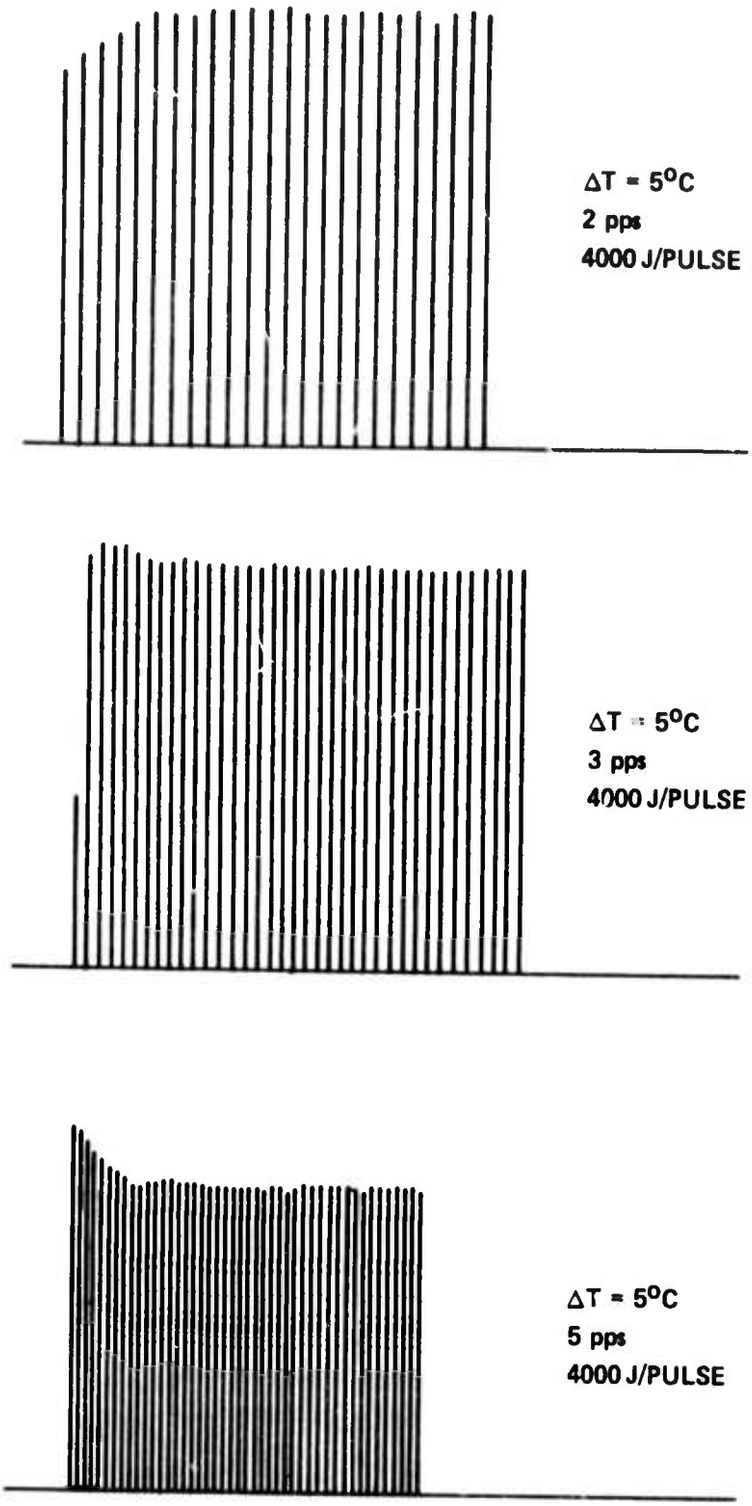

Figure 19. Three Typical Pulse Trains of Laser Output Energy vs. Time for the Same Initial Temperature Difference ΔT and Input Energy per Pulse. Pulse repetition rate variable.

give the same average output energy as a smaller input energy more frequently repeated, even though the average input power is the same. Clear departures are usually characteristic of extremes of input energy and repetition rate. For most of the experiments, however, the average input power is a satisfactory parameter for describing the laser behavior, and it certainly brings out the main trends.

First, we consider the results for the four-lamp quadruple ellipse flash head. For the bulk of this work, an output mirror reflectivity of 52% was used since it was optimum in the sense that it provided a good output coupling with a reasonably low threshold. Three flow speeds, corresponding to Reynolds numbers of 6,000, 8,000 and 10,000 were used. Temperature differentials ranged from 0 to 13°C; the latter was the maximum that could be obtained reliably.

A typical result is shown in Figure 20. The different points at each input power level are the result of different combinations of pulse energy and repetition rate. The latter varied between 0.5 and 5 pps. The curve drawn through these points was the best "eyeball" fit to the average since there does not appear to be a simple analytical expression for the curve. The scatter is typical and in the subsequent graphs, Figures 21 to 24, the points were omitted for clarity.

The prineipal characteristics of these curves are:

1) There is a maximum in E/E_0 corresponding to some input power.

2) As the flow speed increases, the maximum moves to a higher average input power and the maximum value of E/E_0 increases.

3) As the temperature differential increases, the average input power at which the maximum in E/E_0 occurs increases.

4) The extrapolated value of E/E_0 at zero average power input decreases with increasing temperature differential and, for a fixed temperature differential, increases with increasing Reynolds number.

Some of these characteristics can be made more quantitative. In Figure 25, the logarithm of the extrapolated value of E/E_0 is plotted against the temperature differential. For each Reynolds number, the points fall on a straight line. Further, if, as in Figure 26, we plot the input power (P_{max}) at which the maximum in E/E_0 occurs against ΔT on a log-log plot, again a straight line relationship is found. The meaning of these relationships is not yet clear, but we will return later to the results depicted in Figure 25.

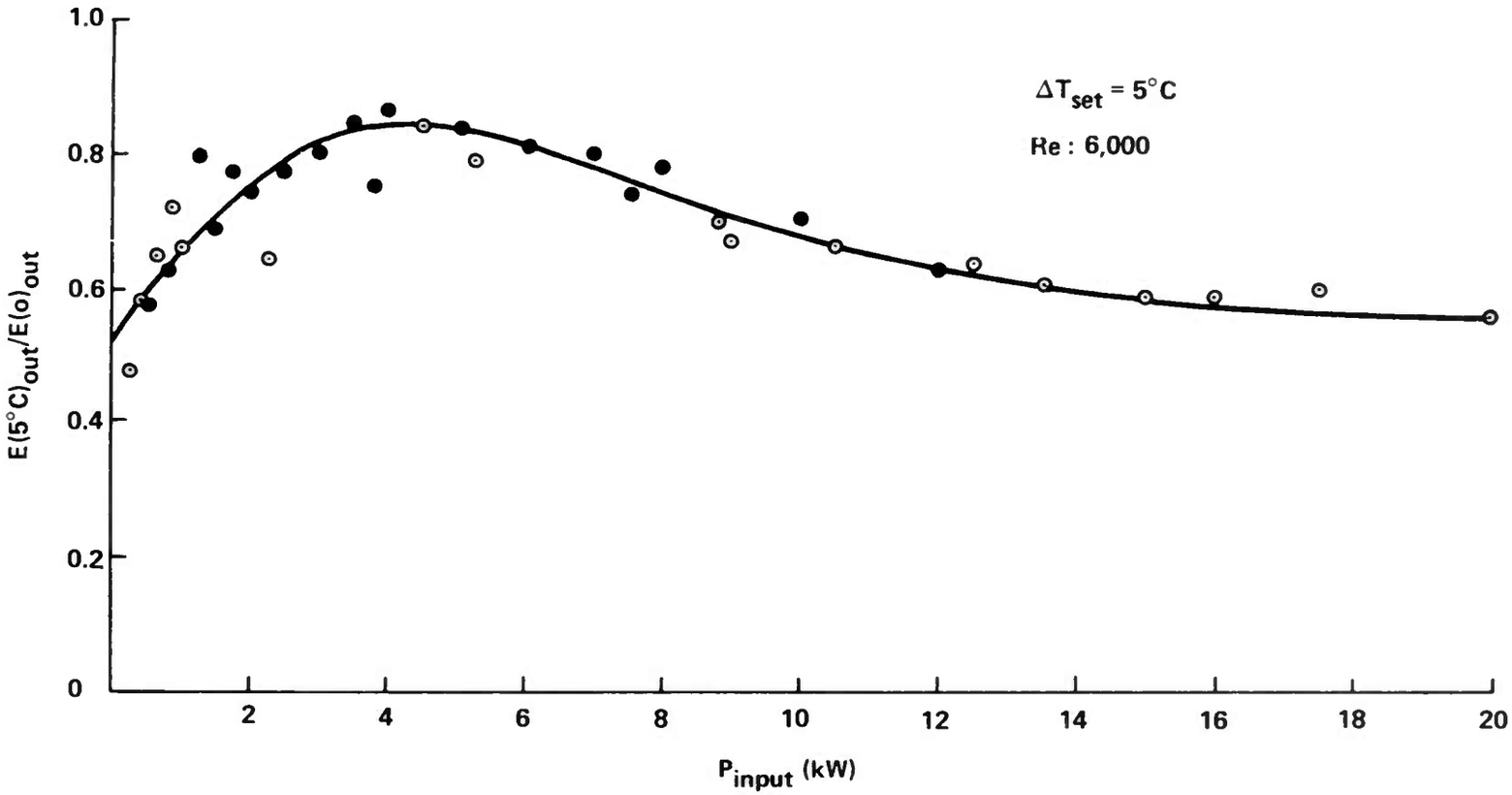

Figure 20. Laser Output for $\Delta T = 5\,^{\circ}C$ Normalized to Single-Shot Output for $\Delta T = 0$ vs. Average Input Power. Reynolds number: 6,000. Data points retained to show scatter.

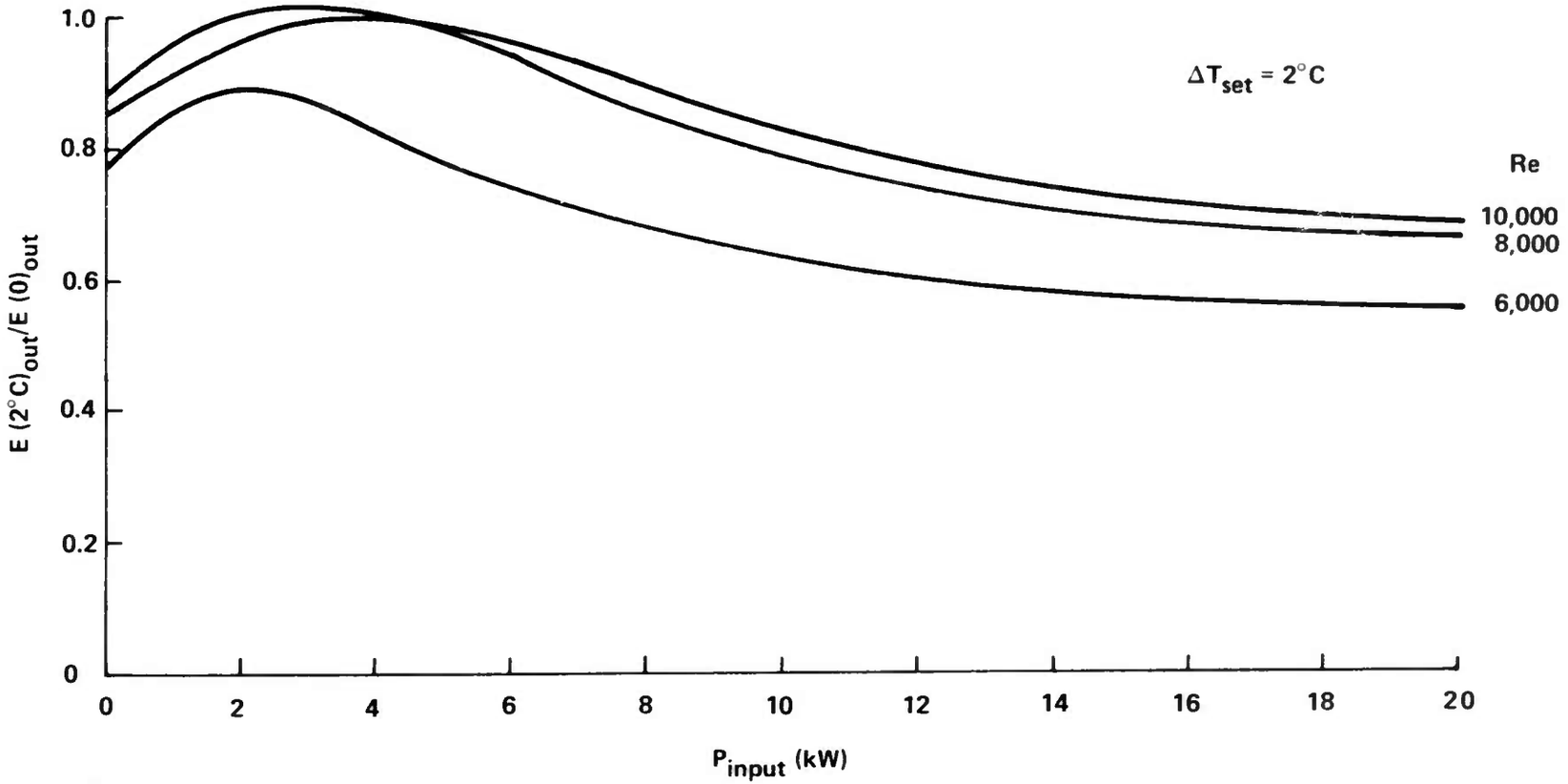

Figure 21. Normalized Laser Output for Four-Lamp 10-Inch Head with $\Delta T = 2°C$ and Re = 6,000, 8,000 and 10,000 vs. Average Input Power. Data points suppressed for clarity.

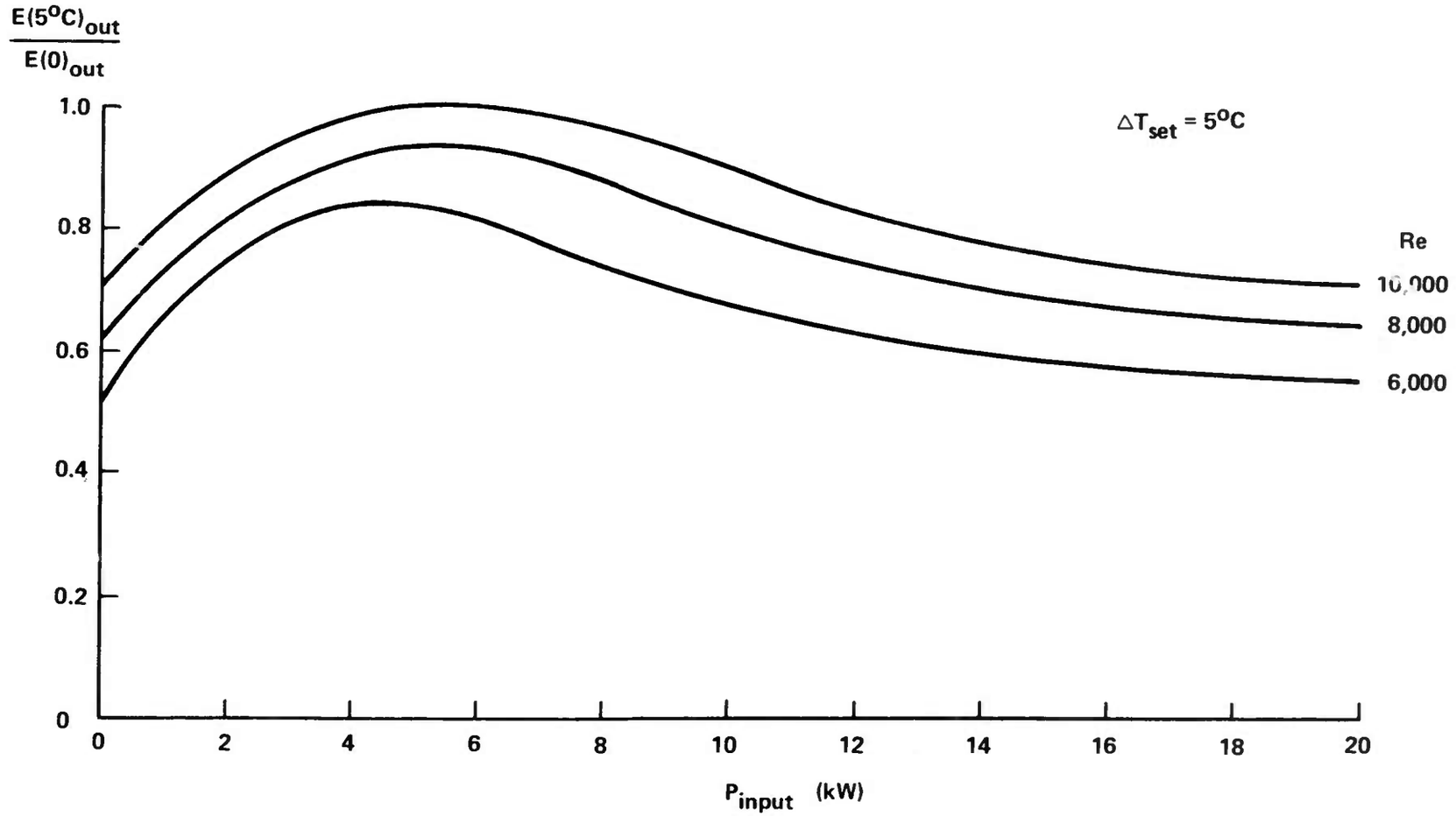

Figure 22. Normalized Laser Output for Four-Lamp 10-Inch Head with $\Delta T = 5\,^{\circ}C$ and Re = 6,000, 8,000 and 10,000 vs. Average Input Power. Data points suppressed for clarity.

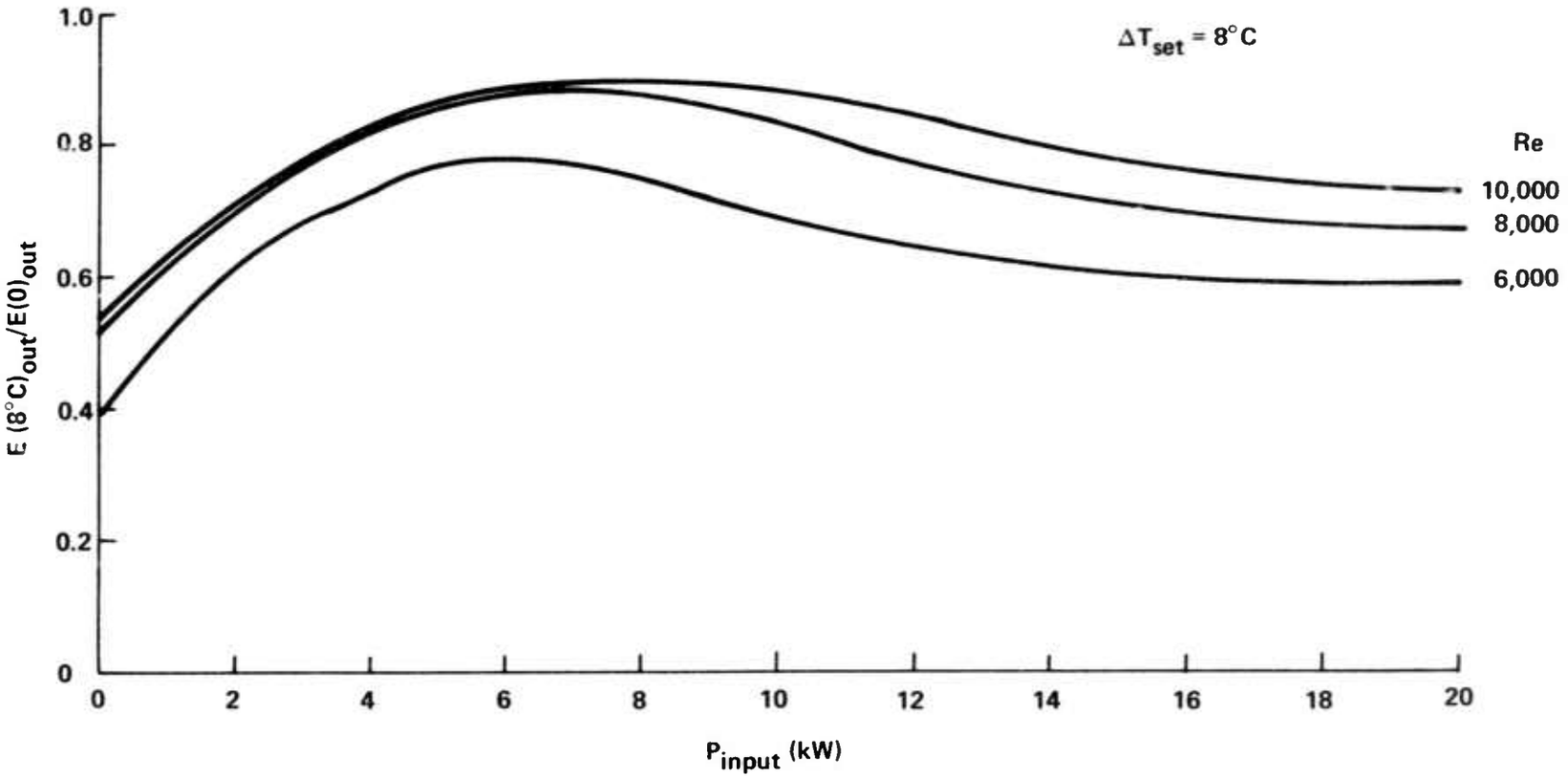

Figure 23. Normalized Laser Output for Four-Lamp 10-Inch Head with $\Delta T = 8\,^{\circ}C$ and Re = 6,000, 8,000 and 10,000 vs. Average Input Power. Data points suppressed for clarity.

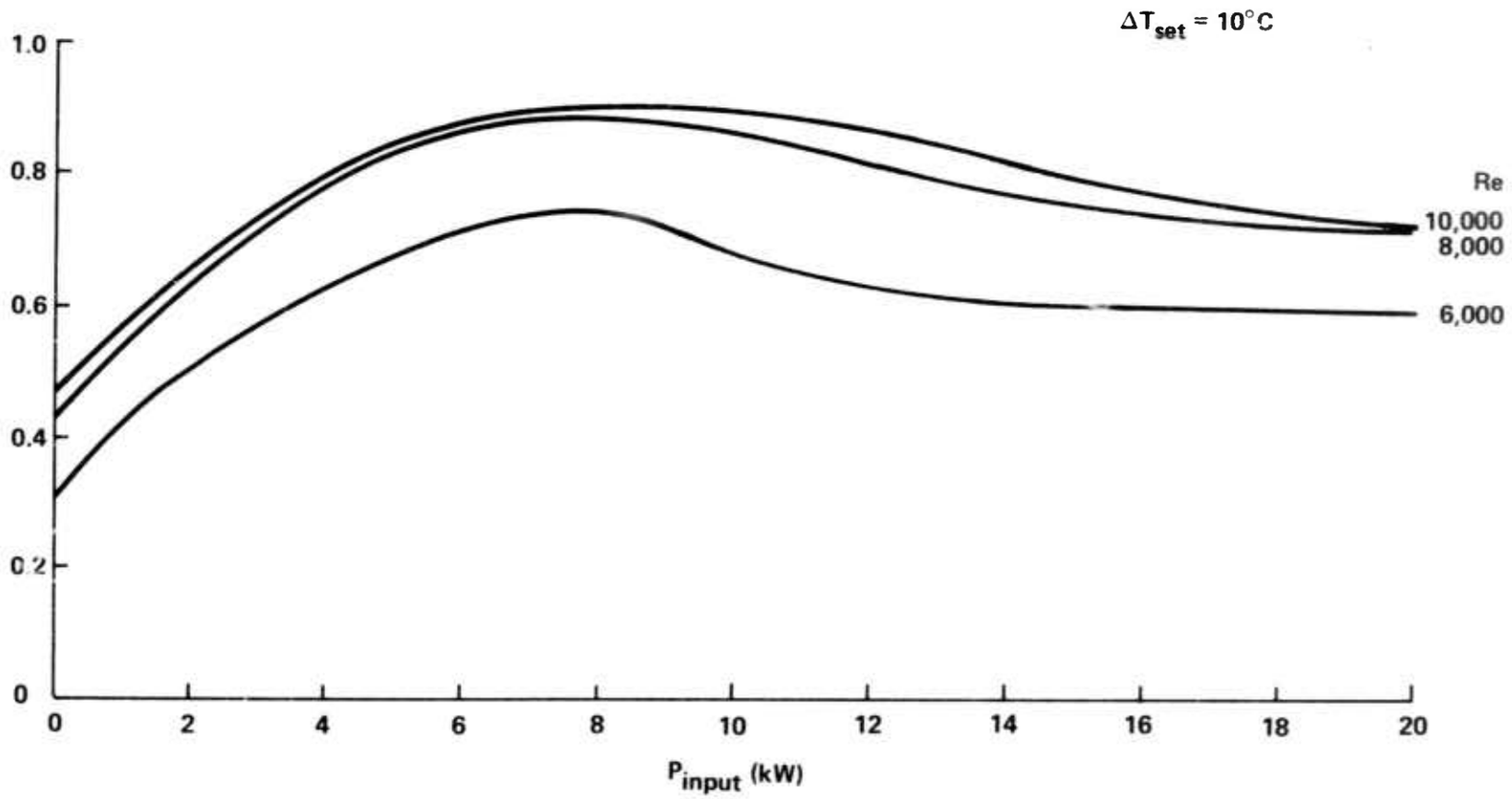

Figure 24. Normalized Laser Output for Four-Lamp 10-Inch Head with $\Delta T = 10^{\circ}C$ and Re = 6,000, 8,000 and 10,000 vs. Average Input Power. Data points suppressed for clarity.

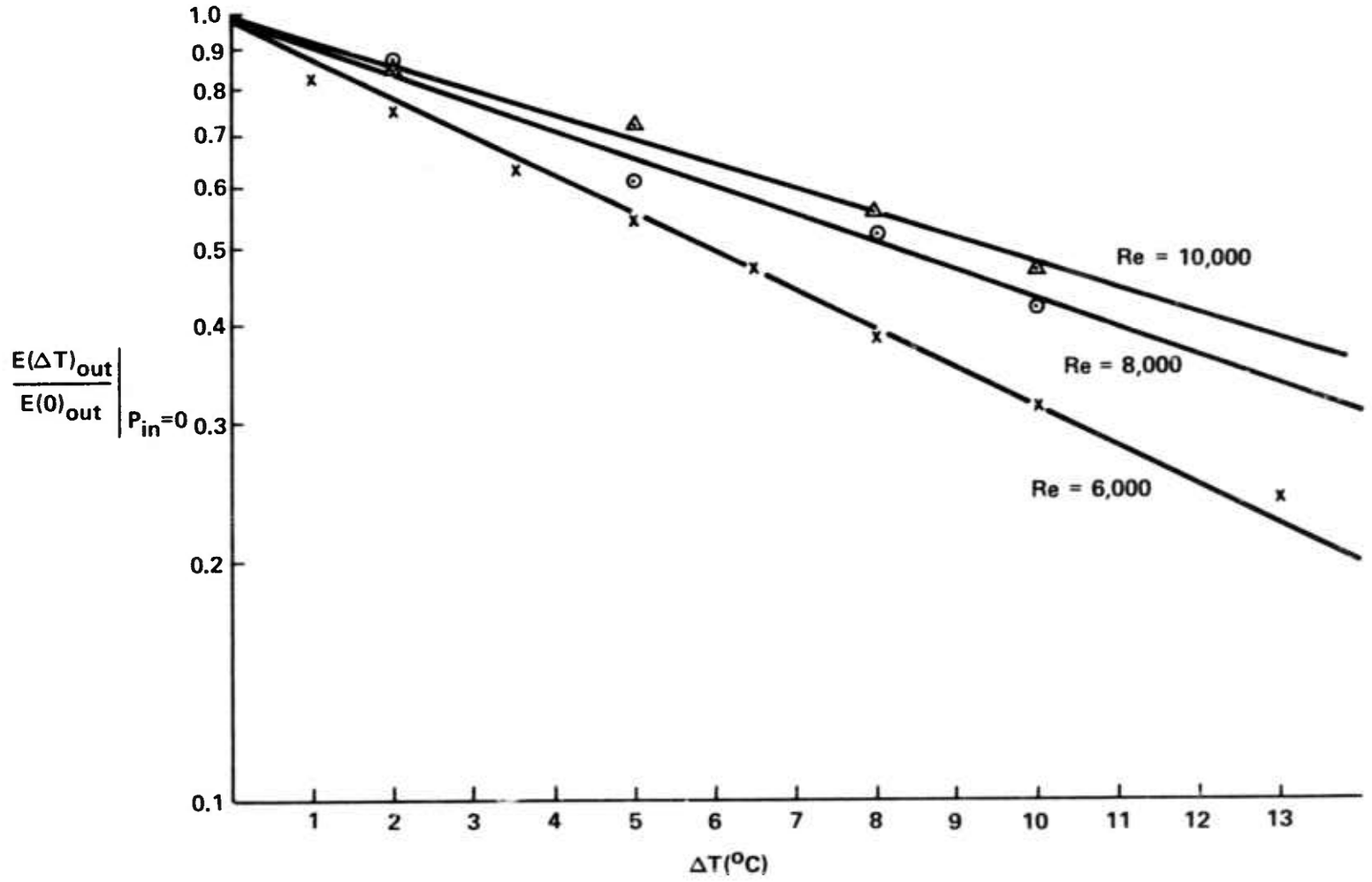

Figure 25. Normalized Laser Outputs Extrapolated to Zero Average Input Power vs. ΔT for Four-Lamp 10-Inch Head. Re = 6,000, 8,000 and 10,000.

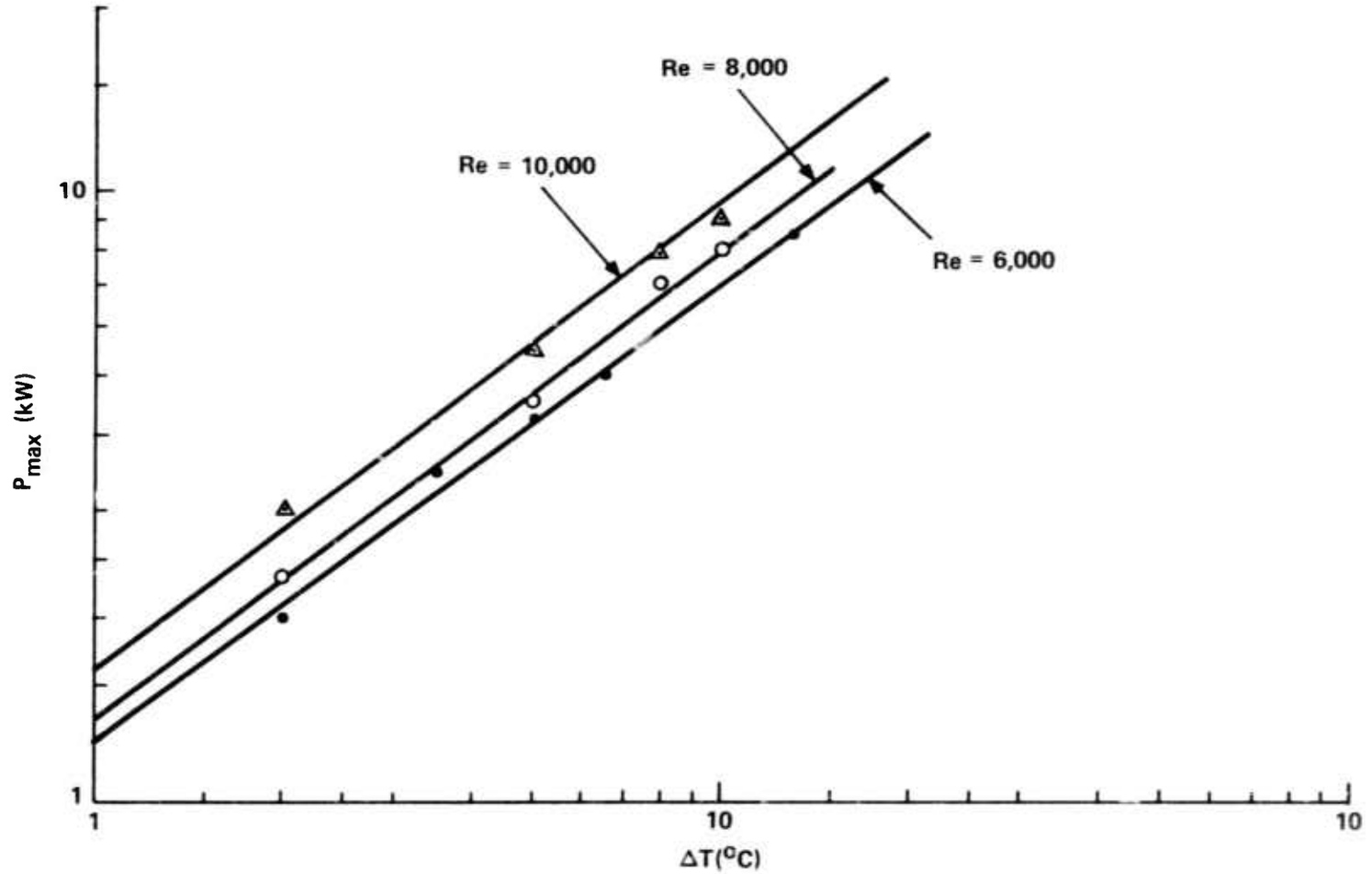

Figure 26. Average Input Power at Which Normalized Laser Output is Maximized (P_{max}) vs. ΔT for Four-Lamp 10-Inch Head. Re = 6,000, 8,000 and 10,000.

The intermediate cell has an active volume half that of the four-lamp head discussed above. Since only two flash lamps were used with this cell, and since each was used with the same energy loading, one would expect similar output for similar input. As seen in Figure 27, this is very nearly the case. Thresholds are slightly lower for the smaller cell, probably because the center of the cell is more efficiently pumped. The curvature in the output at the high pumping part of the curve is probably a result of the higher flux density in the smaller cell. This effect is similar to the curvature seen in the high output mirror reflectivity case illustrated in Figure 15. The loss measurements made on this cell fall within the range of those obtained for the larger cell.

On repetitive pulsing with varying temperature differentials, the results are qualitatively the same as those for the large cell, but differ quantitatively. Figures 28 and 29 show the dependence of E/E_0 on the average input power for temperature differentials. The qualitative observations made earlier for the larger laser are applicable in toto to the present case. In general, however, the behavior of this laser is more sensitive to changes in temperature and the maximum values of E/E_0 more nearly approach unity. In addition, as Figures 30 and 31 show, the details of characterization given in Figures 25 and 26 are different in the present case. In the case of Figure 30, a single linear relationship is not valid over the entire temperature range. There is an abrupt change for the relatively small 1.5°C temperature differential and another slower variation over the remainder of the temperature range studied. The slopes in the slowly varying part are similar for the two lasers. Figures 26 and 31 both show a linear relation with the same slopes. The data on the smaller head, when compared to the larger one, appears to correspond to very much higher Reynolds numbers even though the calculated Reynolds numbers are, at least comparable.

5.4 DISCUSSION

We have developed a quantitative hydrodynamic model (Sections 2 and 3) which ultimately provided an expression for the radial thermal gradient and, consequently, the radial refractive index gradient in turbulent pipe flow. We have also carried out laser experiments under controlled thermal conditions. The model should provide some insight into the laser behavior of the system. The model strictly relates to steady fully-developed flow with the flowing medium and the tube wall maintained at fixed temperatures. The hydrodynamic model has not yet been extended to include an external heat source in the region under analysis. An operating laser must function with such a heat source. Thus, a quantitative correlation between the model and the experiment cannot readily be made.

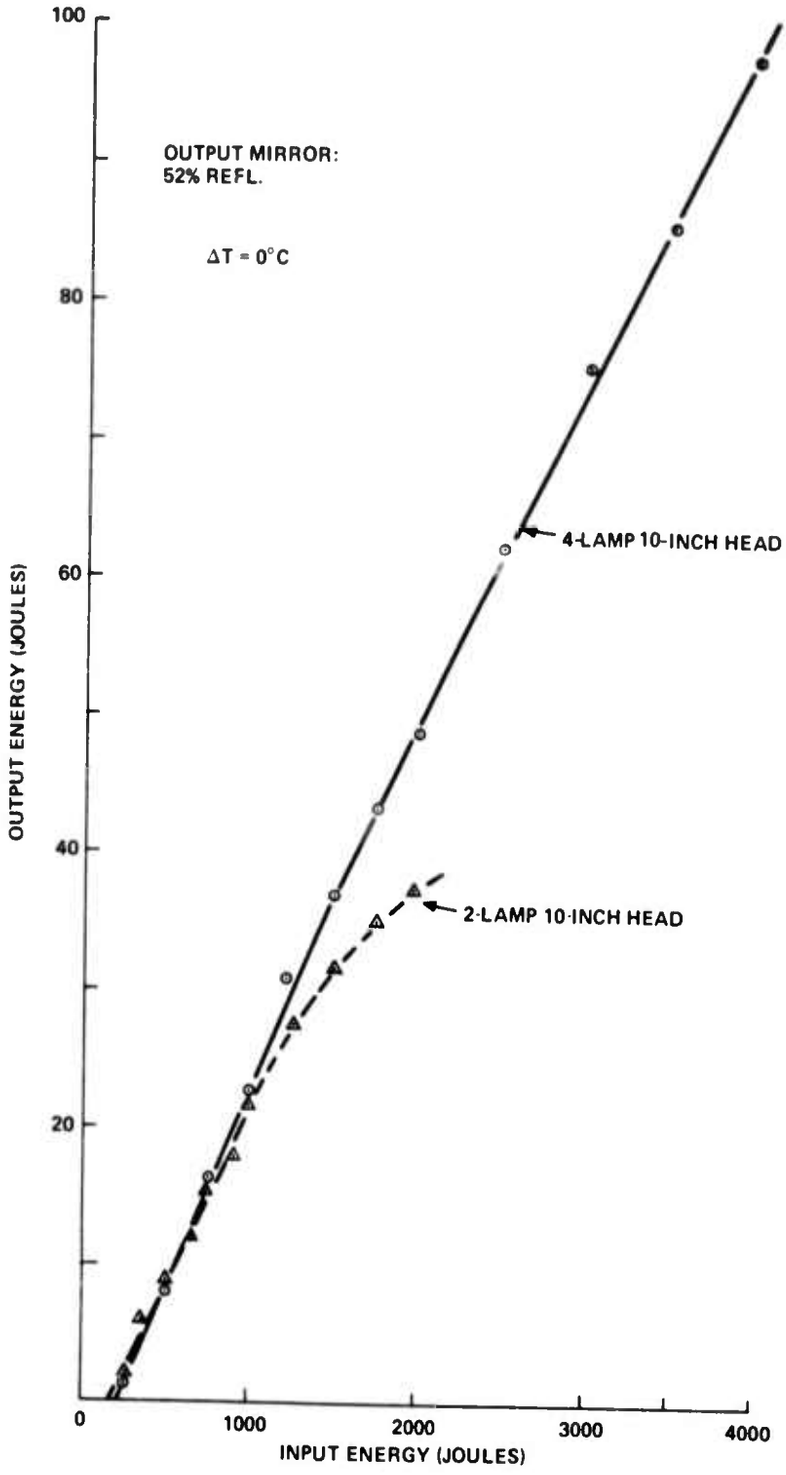

Figure 27. Output Energy vs. Input Energy for Two Largest Laser Heads with $R_{out} = 0.52$ and $\Delta T = 0$. Re for four-lamp head = 6,000. Re for two-lamp head = 8,400.

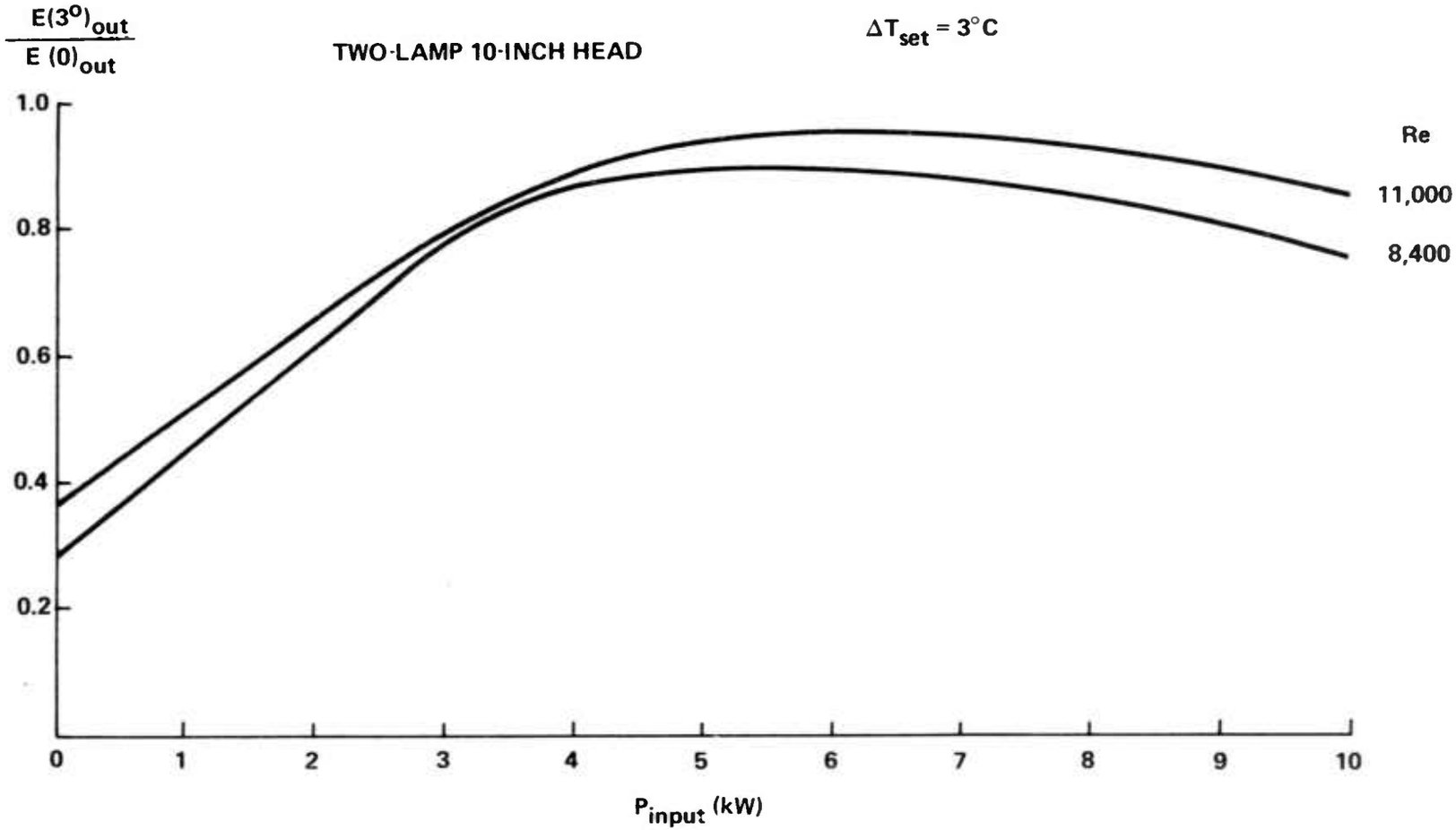

Figure 28. Normalized Laser Output for Two-Lamp 10-Inch Head with $\Delta T = 3°C$ and Re = 8,400 and 11,000 vs. Average Input Power. Data points suppressed for clarity.

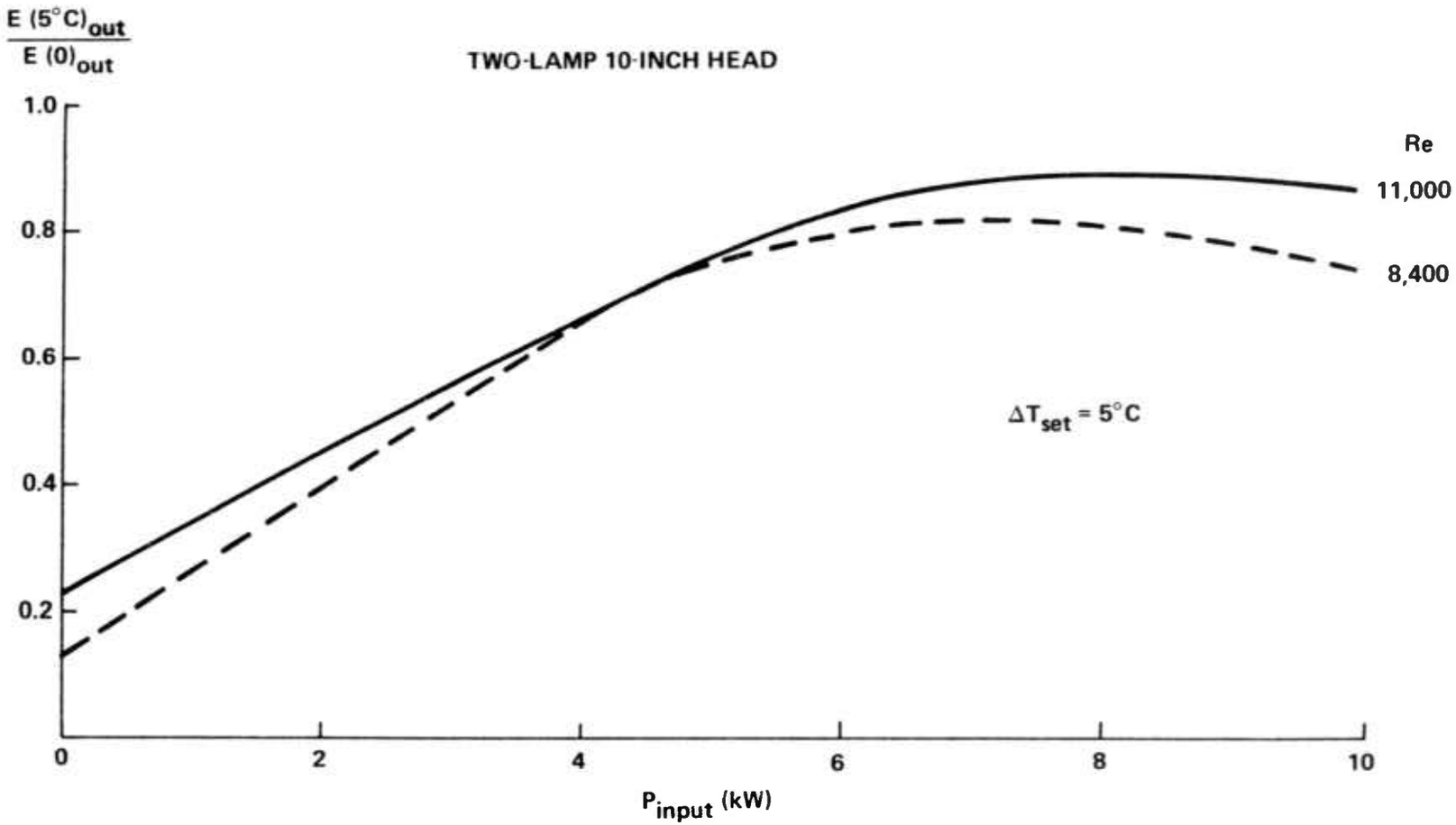

Figure 29. Normalized Laser Output for Two-Lamp 10-Inch Head for $\Delta T = 5^{\circ}C$ and Re = 8,400 and 11,000 vs. Average Input Power. Data points suppressed for clarity.

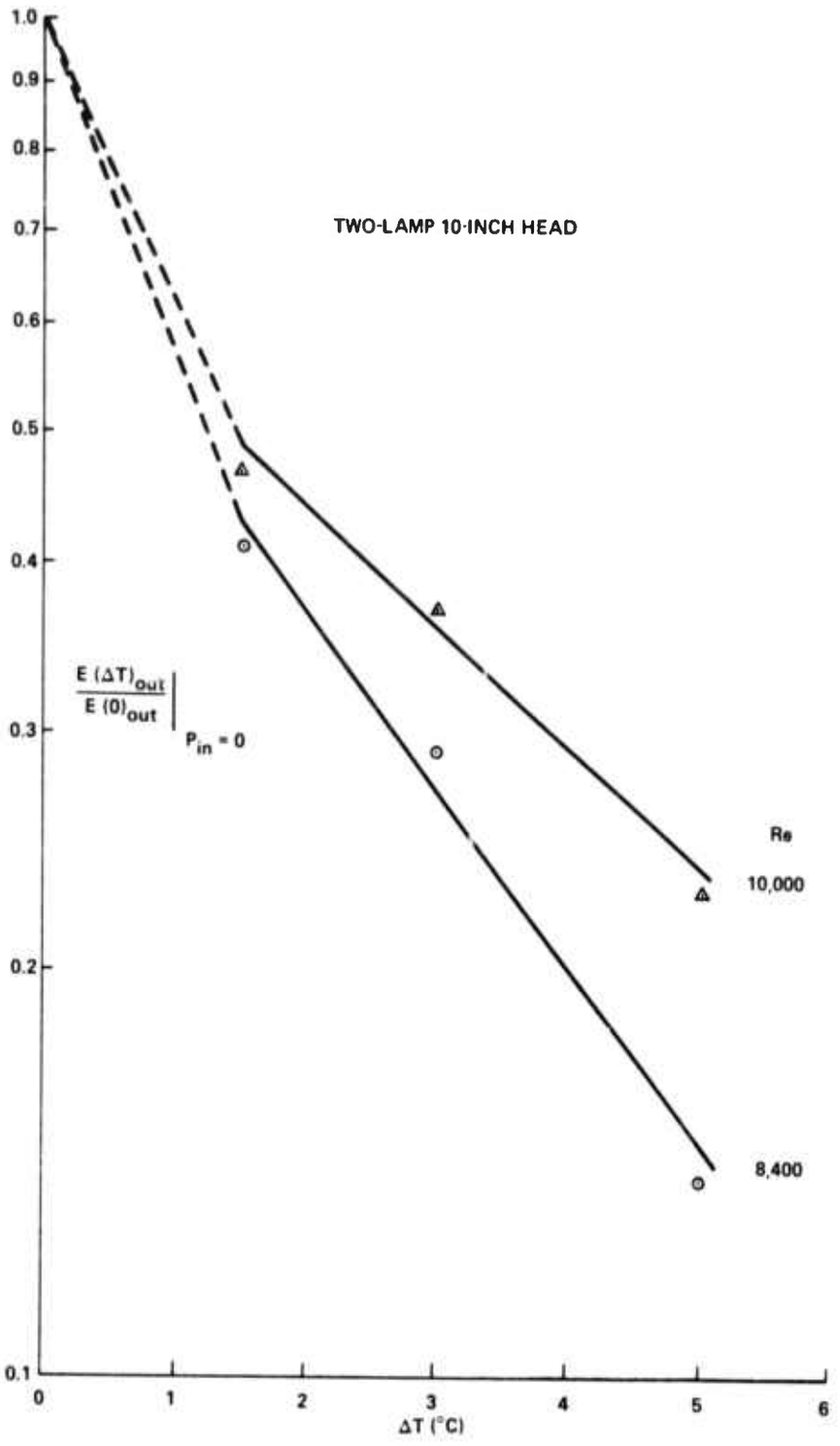

Figure 30. Normalized Laser Outputs for Two-Lamp 10-Inch Head Extrapolated to Zero Average Input Power vs. ΔT for Re = 8,400 and 11,000.

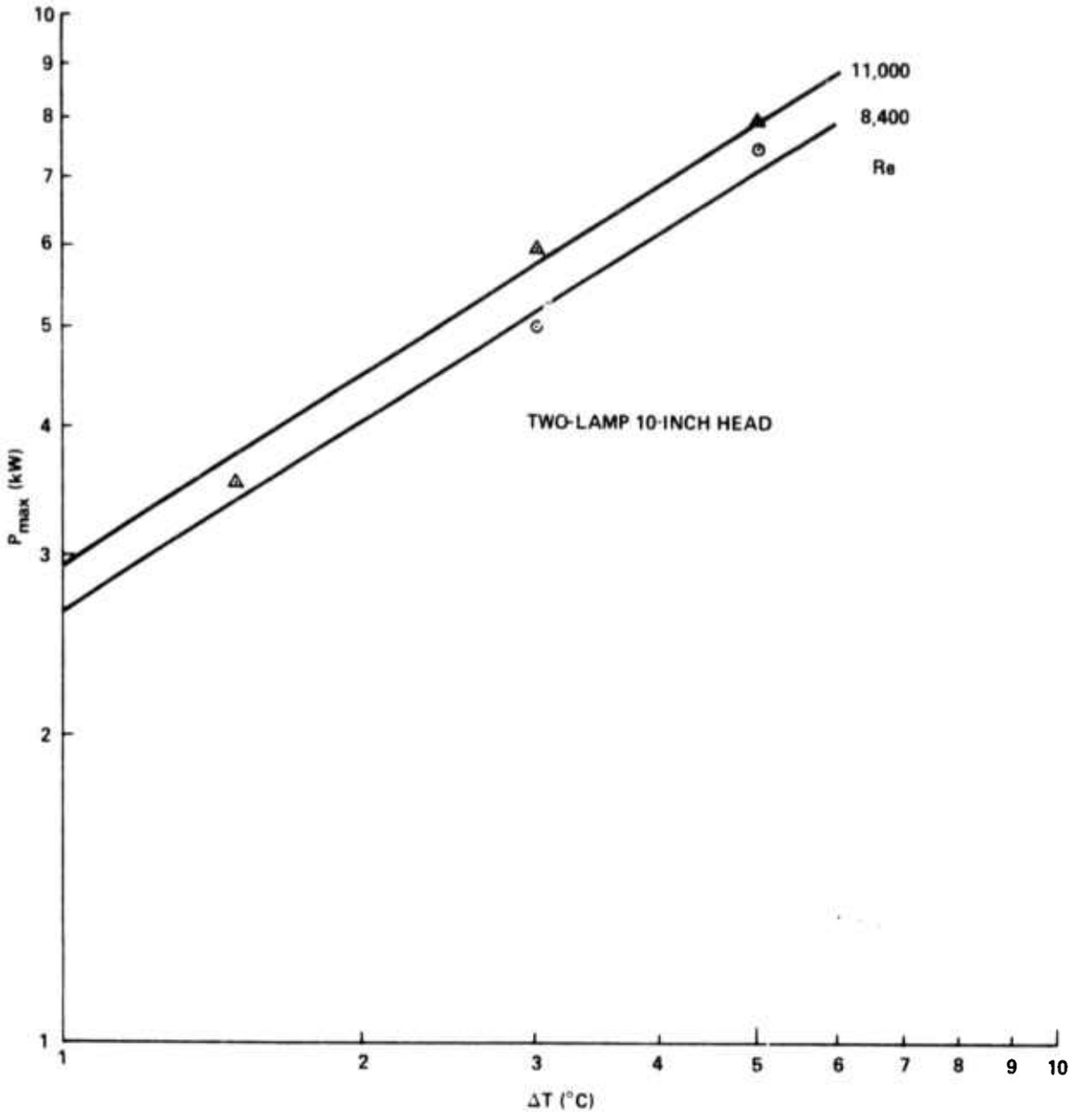

Figure 31. Average Input Power at Which Normalized Laser Output is Maximized P_{max} vs. ΔT for Two-Lamp 10-Inch Head. Re = 8,400 and 11,000.

There is one set of conditions where such correlation is possible, and that is the laser output extrapolated to zero input power. Under other conditions we can use the results of the model as a qualitative guide to understanding the laser behavior. In this section we will correlate the model and the experiment and attempt to explain the main features of the repetitively pulsed laser.

5.4.1 Zero Power Input Results

The zero power input results, Figures 25 and 30, can be understood in terms of the hydrodynamics. The flow in the tube is divided into three regions: the nearly stagnant laminar layer, the buffer layer, and the turbulent core. Given a ΔT between the liquid centerline and the external pipe wall, there will be a radial temperature gradient across the liquid. As $|\Delta T|$ increases, the gradient increases so that, if we fix our attention at some value of the radius between the center and the wall, the gradient will increase as $|\Delta T|$ increases. Now a ray entering normally at that value of r will be deflected as it propagates along the tube. This deflection will also increase with increasing $|\Delta T|$. At some value of dn/dr, this deflcetion will be great enough so that such a ray will not contribute to the laser output. If we pursue this simple picture, we conclude that the radial refractive index gradient vignettes the apertures of the laser and reduces the effcetive volume.

If we assume that the decrease in E/E_0 is a consequence of this vignetting, then $\left(E/E_0\right)_{P=0} = \left(\frac{r_e}{r_0}\right)^2$, where r_c is the critical radius at which the normal ray is deflected too much. Since this deflection depends only on $\left(dn/dr\right)_{r_c}$, we should find that, at $r_e = r_0\left(E/E_0\right)^{1/2}_{P=0}$ for the various flow and thermal conditions, dn/dr is constant. In Table 3 the values calculated for dn/dr are listed and it is seen that they are reasonably constant and, even more important, they show no trend in relation to flow and thermal conditions.

If we take the mean value for dn/dr at $r = r_c$ from Table 3 and substitute this into Eq. (49) from Section 3, we can cal-ulate the difference in optical path length for rays entering the laser resonator at $r = r_c$ and $r = 0$.

$$\Delta P = P\left(r_c\right) - P(0) = \frac{L^3}{6n_0}\left(1 + \frac{3n_0 d_0}{L}\right) n'\left(r_c\right)^2$$

TABLE 3

VALUES OF CRITICAL RADIUS r_c AND dn/dr AT r_c FROM LONG PULSE LASER DATA AND HYDRODYNAMIC CALCULATIONS

Four-Lamp 10-Inch Laser Head ($r_0 = 1.1$ cm)

$T_{CL} - T_0$ (°C)	Re	r_c (cm)	dn/dr at r_c (cm^{-1})	
3.5	6,000	0.875	1.05×10^{-4}	
5.0	6,000	0.81	0.99×10^{-4}	
6.5	6,000	0.75	1.00×10^{-4}	
8.0	6,000	0.685	1.06×10^{-4}	
10.0	6,000	0.62	1.09×10^{-4}	
13.0	6,000	0.545	1.23×10^{-4}	
5.0	8,000	0.865	0.80×10^{-4}	average = 1.01×10^{-4} cm^{-1}
8.0	8,000	0.80	1.01×10^{-4}	
10.0	8,000	0.72	1.01×10^{-4}	
5.0	10,000	0.94	1.00×10^{-4}	
8.0	10,000	0.815	0.92×10^{-4}	
10.0	10,000	0.76	0.97×10^{-4}	

Two-Lamp 10-Inch Laser Head ($r_0 = 0.80$ cm)

1.5	8,400	0.51	2.02×10^{-4}	
3.0	8,400	0.43	0.35×10^{-4}	
5.0	8,400	0.30	0.46×10^{-4}	
1.5	11,000	0.545	4.22×10^{-4}	average = 1.31×10^{-4} cm^{-1}
3.0	11,000	0.485	0.34×10^{-4}	
5.0	11,000	0.38	0.45×10^{-4}	

where, for these experiments:

L = active length of cell = 25 cm

d_0 = distance between resonator mirror and laser cell = 15 cm

n_0 = nominal index of refraction of liquid = 1.45

$n'(r_c) = 1.11 \times 10^{-4}\ cm^{-1}$ (average of all readings)

$$\Delta P = \frac{(25)^3}{8.7}\left(1 + \frac{(4.35)(15)}{25}\right)\left(1.11 \times 10^{-4}\right)^2$$

$$= \left(1.8 \times 10^3\ cm^3\right)(1 + 2.61)\left(1.23 \times 10^{-8}\ cm^{-2}\right) = 8 \times 10^{-5}\ cm$$

$$= 0.8\ \mu$$

We therefore calculate that the difference in optical path between the center of the laser cell and the cutoff radius r_c at which the laser is self-apertured is equal to about one wavelength. As mentioned previously, this method of measuring the optical distortion in the laser cell includes the effects of flashlamp-induced distortions due to the rapid rise of the flashlamp pump pulse as well as any radial nonuniformity of excitation. These effects are, of course, extrapolated to the case of zero average power input and, therefore, do not include the effects of a long-term buildup of heat deposited in the laser medium.

5.4.2 Laser Behavior Under Power Loading

As has been pointed out, the hydrodynamic-thermal model developed is amenable to experimental comparison only in the case discussed above — zero power input. The principal interest, however, is the behavior of the laser under the condition of substantial input power. Under these conditions we have to resort to a qualitative description.

Starting then from the condition of zero power input, we have seen that the temperature differential results in a radial thermal gradient. As the laser is pumped, power is absorbed by the liquid and a substantial fraction of this power is dissipated thermally in various nonradiative relaxation steps. In the central turbulent core there is significant mixing and, even more, a rapid material exchange between excitation pulses so that the heated liquid is swept out and replaced with a new sample at the same

temperature as the previous one before excitation. However, in the slower moving buffer layer, the liquid volume exchange is not so rapid and, at the time of a succeeding pulse, there may well be a residual thermal history from the prior pulse. This situation is more extreme in the case of the relatively stagnant laminar layer and in the pyrex cell itself. In the case of the latter, the effect is somewhat mitigated by the filtering effect of the water coolant in both the flash lamp and cell jackets and in the relative transparency of the glass.

As the power continues to be applied, the temperature of the liquid layer near the wall increases, and the radial gradient is reduced. In Figure 32, if (a) represents the initial condition, then (b) represents the situation as the laser is pumped. The reduced gradient results in an increased pulse output energy or an increase in E/E_0. Continued increase in input power will ultimately result in a radially isothermal condition across the cell, as shown in (c) of Figure 32. This corresponds to the region where E/E_0 is a maximum. Further increase in input power then leads to a change in the sign of the radial gradient, as shown in (d) of Figure 32, and again leads to a decrease in E/E_0.

The consequences of this qualitative picture can be correlated with various flow and thermal parameters. First, however, the change in sign of the radial gradient is used to explain the shape of the E/E_0 vs. input power. At the low input power side of the maximum, the medium behaves as a diverging lens and the vignetting effect is rather pronounced. On the high input power side of the maximu, the laser medium behaves as a converging lens and the effect on laser cavity stability and E/E_0 is less severe.

The other factors to be considered are the Reynolds number and ΔT. A higher Reynolds number results in a greater degree of turbulence, and the core encroaches closer to the cell wall. The rate of removal of dissipated power is increased and the maximum in E/E_0 shifts to higher input powers. The behavior of E/E_0 with respect to ΔT is easily seen with reference to Figure 32(a) to (d). Since the temperature of the liquid core is constant, the change in ΔT simply moves the inner wall temperature consistent with changes in ΔT. Thus, the maxima in E/E_0 will occur at lower input powers for smaller values of ΔT.

5.5 SUMMARY

In this section we have presented data on the long pulse performance of the inorganic liquid laser in terms of the Reynolds number of the flow, the temperature

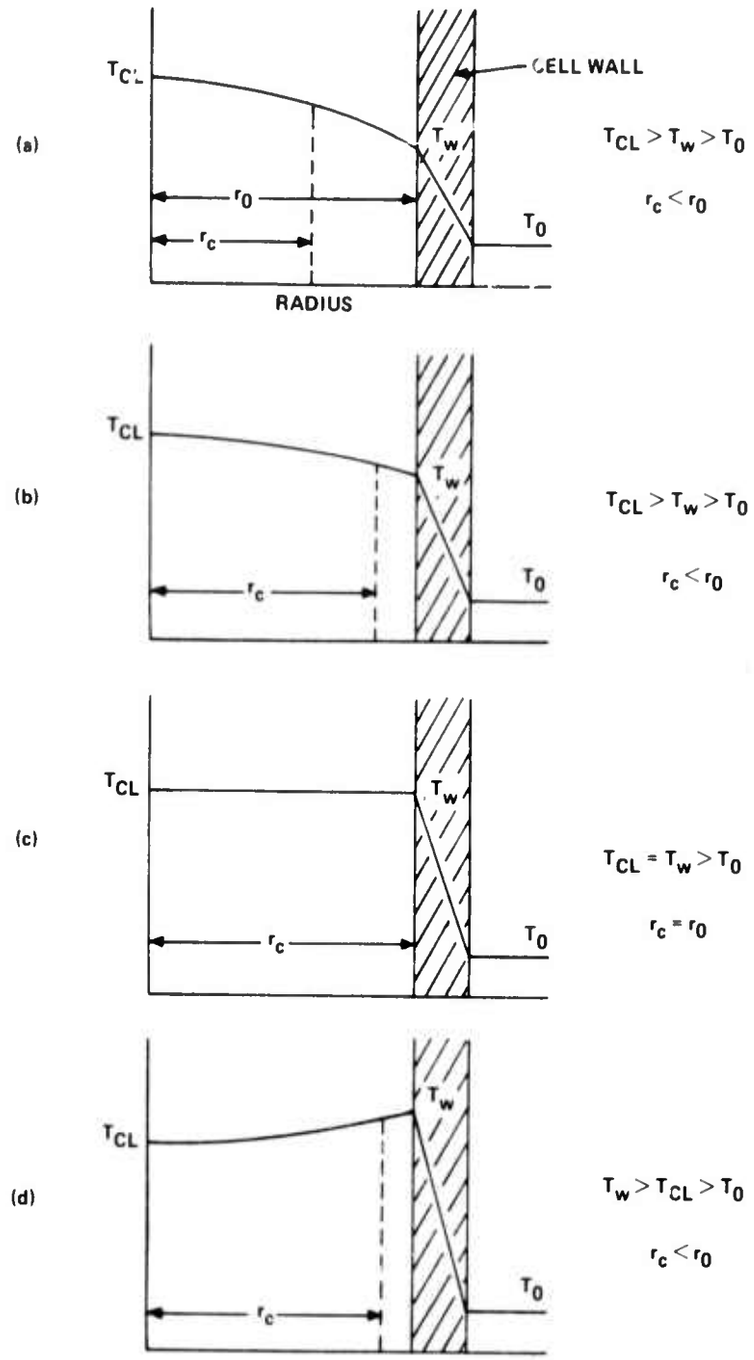

Figure 32. Radial Temperature Profiles Aeross a Water-Jacketed Liquid Laser Cell for $\Delta T = T_{CL} - T_0$ and Re Constant Under Four Conditions of Average Input Power. (a) $P_{input} = 0$. (b) $0 < P_{input} < P_{max}$. (c) $P_{input} = P_{max}$. (d) $P_{input} > P_{max}$. The radius r_e is the critieal radius at which a ray entering the laser medium will be defleeted out of the resonator eavity as explained in the text.

difference between the laser liquid and the external water coolant and the input power. It was shown that the system is described reasonably in terms of average input power as the independent variable and E/E_0 as the dependent one.

The behavior at zero input power was correlated phenomenologically with the hydrodynamic-thermal model set up in Sections 2 and 3. The laser liquid was characterized by a radial thermal gradient and the optical consequences of this gradient were shown to be the deflection of a ray that was initially parallel to the optic or cylinder axis. Such ray deflection could be interpreted in terms of a vignetting of the laser aperture and this vignetting was characterized by a particular value of the refractive index gradient, dn/dr.

At higher input powers, a qualitative model was presented describing the changes in the refractive index gradient to be expected under conditions of increasing input power. In terms of this model, the power dependence of the parameter E/E_0 was qualitatively explained. This also included the behavior with respect to ΔT and Reynolds number.

From the data at zero input power, an important piece of information with regard to amplifier performance was obtained. It was shown that, at the radial point where the laser vignetted, the value of dn/dr was such that the change in optical path between the central axial ray and the ray at the critical radius was one wavelength. The beam distortion across this area would then be very small in a single pass.

6. FUTURE PLANS

After the completion of the oscillator work on the two 10-inch lasers, the laboratory was relocated in its new and permanent quarters. This required all of our effort for a period of time, but we are now ready to resume the work.

The first task is to complete the long pulse oscillator work on the third laser head, a double elliptical enclosure containing a 1/2-inch diameter cell of 6-1/2-inch active length. This work will provide small signal gain data, as well as information on the thermal behavior of the laser. Such information is needed when this laser is used as a Q-switched oscillator or preamplifier.

Following this, we plan to concentrate on the amplifier performance. We will investigate the behavior of each laser as an amplifier in both the small signal and gain saturated regimes. At first, single-shot type of experiments will be performed, but information in the repetitive pulsed mode will also be obtained. The data from these experiments will be used to determine the appropriate operating conditions for the oscillator amplifier chain. Both YAG and a liquid Q-switched oscillator will be used to drive the amplifiers.

Since beam quality is a very important feature in the objective of this project, the distortion of the beam will be carefully measured. To do this, we will use the method of Whitehouse et al.[15] for which the equipment has been obtained and set up. We shall endeavor to distinguish between thermally induced distortion and gain distortion.

Our minimum objective is to obtain the design information for the oscillator-amplifier, define its performance limitations and demonstrate its feasibility.

7. REFERENCES

1. G. Benedetti-Michelangeli and S. Martelucci, Applied Optics 8, 1447 (1969).
2. W. M. Rohsenow and H. Choi, Heat, Mass and Momentum Transfer, Prentice-Hall, Inc., Englewood Cliffs, N. J. (1961).
3. T. Von Karman, Trans. ASME 61, 705 (1939).
4. R. C. Martinelli, Trans. ASME 69, 947 (1947).
5. M. Jakob, Heat Transfer, Vol. 1, p 134, John Wiley & Sons, N. Y. (1949).
6. M. Jakob, ibid, p 547.
7. E. P. Riedel and G. D. Baldwin, J. App. Phys. 38, 2720 (1967).
8. G. D. Baldwin and E. P. Riedel, J. App. Phys. 38, 2726 (1967).
9. F. W. Quelle, Applied Optics 5, 633 (1966).
10. H. Winston and R. A. Gudmundsor, Applied Optics 3, 143 (1964).
11. G. E. Devlin, J. McKenna, A. D. May and A. L. Schawlow, Applied Optics 1, 11 (1962).
12. W. R. Scoy and M. L. Stitch, J. App. Phys. 34, 1719 (1963).
13. High Energy Pulsed Liquid Laser Semiannual Technical Summary Report, 28 Feb. 1972.
14. H. Samelson, R. Kocher, T. Waszak and S. Kellner, J. App. Phys. 41, 2459 (1970).
15. D. R. Whitehouse, C. F. Luck, C. P. von Mertens, F. A. Horrigan and M. Bass, 1973 Conference on Laser Engineering and Applications, paper 8.7.